CHAPTER 1

Coherent Backscattering and Anderson Localization of Light

Christof M. Aegerter and **Georg Maret**

Fachbereich Physik, Universität Konstanz, Universitätstrasse 10, 78457 Konstanz, Germany

Contents

1. INTRODUCTION

Most of the time, we obtain information on an object by looking at it, that is, we exploit the light that is scattered from it. The spectral and angular distribution of the backscattered (and reflected) light gives us information about the nature of the particles making up the object. For instance, the reddish color of copper is determined by the absorption properties (in the green) of the d electrons in the partially filled shell.

Progress in Optics, Volume 52 © 2009 Elsevier Science
ISSN 0079-6638, DOI 10.1016/S0079-6638(08)00006-1

On the other hand, the blue color of the sky is well known to originate from the scattering properties of the air molecules, which follows Rayleigh scattering with a cross-section proportional to $1/\lambda^4$. This tells us that the molecules are much smaller than the wavelength of light. In fact, a more thorough analysis allows a characterization of the density fluctuations of the air from the scattering properties of the sky. As a final example, we mention the 'Glory', the halo sometimes seen around the shadow of an airplane on clouds it is flying over, which will be discussed further below. In the following, we will be concerned with instances of such enhanced backscattering in nature, where the intensity is enhanced in the direction of backscattering. As we will see below, one such effect is due to the interference of multiple scattering paths in disordered media like clouds, milk or white paint. Due to the reciprocity of light propagation, such paths will always have a counterpart of exactly the same length, which implies that they will always interfere constructively in the backward direction.

We will also discuss how this effect can lead to a marked change in the transport behaviour of the light waves in a disordered system, where diffuse transport comes to a halt completely. This transition is known as Anderson localization, and has been of great influence in the development of the theory of electrons in metals and condensed-matter physics. However, as will be seen in the discussion of backscattering enhancement below, the effect is also present in classical waves such as light, and there have been great efforts to try and experimentally observe the transition to Anderson localization of light.

In the rest of the introduction, we will discuss the different instances of enhanced backscattering in nature and their possible connection to coherent backscattering. Then we will discuss the connection of coherent backscattering to Anderson localization in more detail, before discussing the main predictions of Anderson localization in order to guide the experimental search for the effect.

Section 2 will return to coherent backscattering and will discuss in detail the different experimental observations connected to recurrent scattering, the influence of absorption and finite size of the medium, as well as the problem of energy conservation. In that section we will also discuss other instances of coherent backscattering, that is, with light scattered by cold atoms as well as with waves other than light.

In Section 3 we will discuss the quest for Anderson localization of light, describing the different experimental approaches used in the past, as well as their advantages and disadvantages. Finally, we will concentrate on our studies of time-resolved transmission and the corresponding determination of critical exponents of Anderson localization of light.

1.1 Instances of Enhanced Backscattering

As first realized by Descartes (1637), the rainbow is an enhancement in intensity (different for different colors due to dispersion) due to refraction of light in the rain drops, which, due to the dispersion of water, is highest at different angles for different colors. However, this is a purely geometric effect, which does not yield information on the size of the rain drops reflecting the light. Something akin to a rainbow can be seen when flying in an airplane over an overcast sky. When the sun is low and the cloud cover not too thick, one can see a beautiful halo around the shadow of the plane on the clouds. The effect is also well-known to alpinists who can observe this halo around their own shadow on a day that is hazy in the valley. In contrast to what one might think, this 'Glory' as it is called, is not in fact a rainbow. One can see this for instance by considering the angle of this colorful enhancement, which is usually only a few degrees and hence much smaller than the 42° corresponding to a rainbow. Therefore another mechanism has to be at work. It has been shown that the size of the scattering droplets influences the angle of the glory (Bryant and Jarmie, 1974). It turns out that this is due to the Mie-scattering properties (Mie, 1908) of the droplets. With a typical size of 10 μm, the droplets in a cloud are large compared to the wavelength of light. Furthermore, as illustrated by experiments on a levitating droplet of water, Glory is the property of a single drop (Lenke, Mack and Maret, 2002).

Enhanced backscattering is also commonly observed in forests, where the leaves of dew-covered trees, or the blades of dew-covered grass, have a halo. This effect is called sylvanshine (see e.g. Fraser (1994)) and is due to the focusing action of the droplet on the reflecting surface of the leaf. By the same principle, the diffuse reflection from the leaf is channeled back through the lens (i.e. the drop) which decreases the angle of reflection. Hence the leaves or the grass blades are brighter than the background. The grass does not even need to be dew-covered to observe a halo, as there is an additional effect increasing the intensity in the direct backscattering direction. Exactly opposite to the incidence, any ensemble of rough objects will be brightest. This is because in this direction, we see the reflected light directly and none is lost due to shadows of other objects (Fraser, 1994). This is known as the corn-field effect.

As a final instance of enhanced backscattering, let us mention observation of the intensity of objects in the solar system, such as the moon or other satellites of planets, when the earth and the sun are in opposition to the moon. In that case, it was observed by Gehrels (1956) for the moon and subsequently for many other satellites (Oetking, 1966) that the intensity of the satellite is in fact increased over its usual value. Due to the arrangement of sun and satellite when the effect is observed, this was called the 'opposition effect'. In this effect, coherent backscattering as we will discuss below, works in concert with analogues of the effects

described above, such as the corn-field effect. The presence of coherent backscattering in the opposition effect was discovered (Hapke, Nelson and Smythe, 1993). With this knowledge it was then possible to actually study the surface properties (e.g. the granularity) of these satellites from remote observations.

1.2 Coherent Backscattering

Among instances of enhanced backscattering, here we will be concerned mostly with coherent backscattering, an interference effect that survives all averages in a random medium. Fundamentally, the enhancement is due to the fact that, because of time-reversal symmetry, every path through a random medium has a counterpropagating partner. Light elastically scattered on these two paths interferes constructively, because the path-lengths are necessarily the same. This leads to an enhancement of exactly a factor of two in the direction directly opposite to the incidence. In contrast to Glory or other effects discussed above (Lenke, Mack and Maret, 2002), coherent backscattering is not an interference due to the properties of a single scatterer, but relies fundamentally on multiple scattering. In fact, in the single-scattering regime there cannot be a coherent backscattering cone as there cannot be a counterpropagating light path. The entry- and exit-points of a multiple-scattering path can then be seen as the two points of a double slit, which, due to the coherence of the time-reversed paths, necessarily interfere with each other. The different interference patterns corresponding to different light paths in the disordered medium have to be averaged over, which will lead to the shape of the backscattering cone discussed in Section 1.3 below. What can be seen from this picture is that in the exact backscattering direction, the averaging will always lead to an enhancement factor of two.

These principles behind the origin of the backscattering cone will strongly influence the transport through a random system. Taking the end points of the counterpropagating paths to coincide somewhere inside the sample, there will be a two-fold enhancement at this point on such a closed loop. This in turn leads to a decreased probability of transport through the system. This effect is what causes Anderson localization of light (Anderson, 1958), i.e. the loss of diffuse transport due to increasing disorder. As disorder increases, the probability of forming closed loops on which intensity is enhanced increases. At a certain critical amount of disorder, these closed loops start to be macroscopically populated, which leads to a loss of diffuse transport. This critical amount of disorder has been estimated using dimensional arguments by Ioffe and Regel (1960) to be when the mean free path roughly equals the inverse wavenumber, i.e. when $kl^* \sim 1$. Such a mechanism was first proposed for the transport of electrons in metals, where it was found that an increase in disorder can turn a metal into an insulator (see e.g. Bergmann (1984)).

Historically, the first instances of localization were discussed in the context of electron transport in metals, and thus localization was thought to be a quantum effect. Moreover, due to the fact that localization should always be present in two dimensions (see scaling theory below) and is not influenced too much by the presence of correlations, these studies were carried out in thin films. A review of these experiments can be found in Altshuler and Lee (1988) and Bergmann (1984) and these studies of localization in lower dimensions have had a big influence on the study of other quantum effects in low-dimensional electron systems, such as the quantum Hall effect (Klitzing, Dorda and Pepper, 1980; Laughlin, 1983).

Eventually however, it was realized that the quantum nature of electrons is not a necessary ingredient for the occurrence of Anderson localization as, in fact, this is purely a wave effect. Thus, it should also be possible to observe localization effects with classical waves, such as light, as was proposed by John (1984) and Anderson (1985). As we will see below, coherent backscattering, that is, weak localization, was observed with light shortly thereafter; subsequently, there was a vigorous programme to also observe signs of strong localization of light, because the study of photon transport in disordered media has many advantages over the study of electrons in metals. This is because in the latter case there are alternatives that may also lead to localization: in the case of electrons, a random potential can lead to a trapping of particles, which also strongly affects transport, while not being connected to localization. On the other hand, electrons also interact with each other via Coulomb interaction, so that correlations in electron transport are again not necessarily due to localization effects, but may more likely be explained by electron–electron interactions. In fact, it can be shown that in the presence of particle interactions, the effects of localization vanish (Lee and Ramakrishnan, 1985).

However, as we will discuss below, the photonic system is not completely free either of possible artifacts masking as localization. For instance, light will be absorbed by materials to a certain extent, which leads to a loss of energy transport similar to localization. Furthermore, resonant scattering can lead to a time delay in the scattering process, which leads to a slowing down of transport, which again may be mistaken for localization. In Section 3 we will discuss in detail how these possible artifacts can be circumvented and localization can in fact be observed.

1.3 Theoretical Predictions

As discussed above, the enhanced backscattering from turbid samples, known as coherent backscattering, is a manifestation of weak localization of light. Localization has been studied intensely in electronic systems, and many of the predictions found there can be applied also to optics. Here we will discuss the most important predictions, which will also

serve as a guiding line in the quest to observe Anderson localization of light. Most prominent in these are the predictions of the change in static transmission (Anderson, 1985; John, 1984) which turned out to be difficult to observe experimentally due to the presence of absorption in real samples. The critical prediction for Anderson localization concerns the fact that there should be a phase transition to a state where diffusion comes to a halt. This is described by scaling theory (Abrahams, Anderson, Licciardello and Ramakrishnan, 1979), which can also be investigated by a self-consistent diagrammatic theory (Vollhardt and Wölfle, 1980). This version of the theory can also be extended to describe open systems with absorption, a situation much more suitable for experiments (Skipetrov and van Tiggelen, 2004, 2006). First of all, however, we will describe the shape of the backscattering cone as calculated by Akkermans, Wolf and Maynard (1986) and van der Mark, van Albada and Lagendijk (1988).

1.3.1 The Cone Shape

Given the nature of the backscattering cone due to interference of photons on time-reversed paths, one can explicitly calculate the shape of the enhancement as a function of angle. In order to do this, the interference patterns, corresponding to two counterpropagating paths with end-to-end distance ρ, need to be averaged weighted by the probability distribution of such an end-to-end distance occurring. Like in a double-slit experiment with slit separation ρ, each of these interference patterns will contribute a factor $1 + \cos(q\rho)$, such that the enhancement above the incoherent background is simply given by the real part of the Fourier transform of the end-to-end distance distribution:

$$\alpha(q) = \int p(\rho) \cdot \cos(q\rho)\, \mathrm{d}\rho. \tag{1}$$

In the diffusion approximation, this probability distribution can be calculated (Akkermans, Wolf, Maynard and Maret, 1988; van der Mark, van Albada and Lagendijk, 1988) to be $1/a(1 - \rho/\sqrt{\rho^2 + a^2})$ in the case of a semi-infinite planar half-space. Here, the length scale $a = 4\gamma l^*$ describes how the diffuse intensity penetrates the sample as described by the Milne parameter γ and the transport mean free path l^*. The parameter γ can be calculated from the radiative transfer equation to be $\sim$0.71 and in the diffusion approximation is exactly $\gamma = 2/3$. In the following, we will always use the value of $\gamma = 2/3$. This leads to the following expression for the backscattering enhancement:

$$\alpha(q) = \int \left(1 - \frac{\rho}{\sqrt{\rho^2 + a^2}}\right) \cdot \cos(q\rho)\, \mathrm{d}\rho, \tag{2}$$

which can be solved to give (Akkermans, Wolf and Maynard, 1986; Akkermans, Wolf, Maynard and Maret, 1988; van der Mark, van Albada and Lagendijk, 1988):

$$\alpha(q) = \frac{3/7}{(1+ql^*)^2}\left(1 + \frac{1-\exp(-4/3ql^*)}{ql^*}\right). \tag{3}$$

This gives a cone shape in very good agreement with the experiments that will be discussed in Section 2. As can be seen from an investigation of the angle dependence, the cone tip is triangular with an enhancement of 1 in the exact backscattering direction. The enhancement then falls off on an angular scale proportional to $1/(kl^*)$; in fact the full width at half maximum of the curve is given by $0.75/(kl^*)$. Thus the investigation of the backscattering cone is a very efficient method of determining the turbidity of a sample as given by $1/l^*$.

A similar description following diagrammatic theory, where the most crossed diagrams have to be added up, was given by Tsang and Ishimaru (1984). The main features of the curve remain the same, however the different theories use different approximations for the Milne parameter.

1.3.2 Static Transmission

One of the main predictions of Anderson localization in electronic systems is the transition from a conducting to an insulating state. This of course has strong implications for the transmission properties of localized and non-localized samples. For a conducting sample, the transmission is described by Ohm's law, which describes diffusive transport of particles and hence a decrease of transmission with sample thickness as $1/L$. This is also the case in turbid optical samples, where the transmission in the diffuse regime is simply given by $T(L) = T_0 l^*/L$ (see e.g. Akkermans and Montambaux (2006)). In the presence of absorption, this thickness dependence of the total transmission will change to an exponential decay for thick samples according to

$$T(L) = T_0 \frac{l^*/L_a}{\sinh(L/L_a)}, \tag{4}$$

where $L_a = \sqrt{l^* l_a/3}$ is the sample absorption length corresponding to an attenuation length l_a of the material, which describes the absorption of the light intensity along a random scattering path.

The localization of photons will similarly affect the transmission properties of a sample. As the diffusion coefficient of light becomes scale dependent close to the transition to localization, the total transmission will decrease. Scaling theory of localization, to be discussed below, predicts that the diffusion coefficient at the transition will decrease as $1/L$

(John, 1984). This should then be inserted into the expression for the diffuse transmission of the sample, resulting in a different thickness dependence $T(L) \propto 1/L^2$. Again, this ignores the effects of absorption, and Berkovits and Kaveh (1987) have calculated the effects of absorption in the presence of a renormalized diffusion coefficient, finding

$$T(L) = T_0 \exp(-1.5L/L_a). \tag{5}$$

Again, this leads to an exponential decrease of the transmitted intensity for very thick samples, where, however, the length scale of the exponential decrease has changed. When photons are fully localized, the transport is exponentially suppressed, as only the tails of the localized intensity can leave the sample. Thus Anderson (1985) has predicted the transmission in the localized case to be given by $T(L) = T_0 \exp(-L/L_{\text{loc}})$, where L_{loc} describes the length scale of localization. As was the case above, this derivation again does not take into account absorption, and a fuller description would be given by

$$T(L) = T_0 \frac{l^*/L_a}{\sinh(L/L_a)} \exp(-L/L_{\text{loc}}). \tag{6}$$

Again, this gives an exponential decrease of the transmitted intensity for thick samples with an adjusted length scale not solely given by the absorption length L_a. In an experimental investigation of Anderson localization therefore, static transmission measurements will have to find an exponential decrease of the transmission that is faster than that given by absorption alone. This implies that the absorption length must be determined independently for such an investigation to be able to indicate localization of light.

1.3.3 Scaling Theory

When studying the thickness dependence of the conductance (i.e. the transmission), its dependence on disorder has to be taken into account. Abrahams, Anderson, Licciardello and Ramakrishnan (1979) produced the first version of such a theory, where they introduce the 'dimensionless conductance' g as the relevant parameter to study. In electronic systems, this simply is the measured conductance normalized by the quantum of conductance, e^2/h. In optics, the conductance is naturally dimensionless and can be defined simply via the transmission properties of the sample. In fact, g can be calculated in three dimensions from the ratio of the sample volume to that occupied by a multiple scattering path. This volume of the multiple scattering path is given by $\lambda^2 s$, where s is the length of the path, which in the case of diffusion is $s \propto L^2/l^*$. Thus one obtains $g \approx (W/L)(kW)(kl^*)$, where W is the width of the illumination,

which could also be obtained from the static transmission discussed above. In the case of a localized sample, the transmission decreases exponentially with L, which has to be reflected in a renormalization of the path-lengths in order to give an exponentially decreasing g. The main ansatz of Abrahams, Anderson, Licciardello and Ramakrishnan (1979), in treating the problem of the localization transition in the following, is to suppose that the logarithmic derivative $\beta = \mathrm{d}(\ln g)/\mathrm{d}(\ln L)$ can be expressed as a function of g only.

The transition to a localized state is then given by the criterion that β changes from a positive value to a negative one. Ohm's law as a function of dimensionality states that the conductance scales as $g \propto L^{d-2}$. Therefore, making a sample larger and larger in low-dimensional systems will in fact lead to a reduction of the conductance and hence be associated with localization. Actually Ohm's law straightforwardly implies that $\beta = d - 2$ for large L (and thus g), such that $d = 2$ is the lower critical dimension for a transition to localization to occur. In fact, for low-dimensional systems the waves are always localized (Abrahams, Anderson, Licciardello and Ramakrishnan, 1979).

Where there is a transition to localization (i.e. in $d > 2$), more details about that transition can be obtained by assuming the dependence of β on g to be linear at the crossing of the null-line. In this case, the scaling function β describes how one arrives from a diffuse conductance to one which is exponentially suppressed in the localization length. This transition is a function of the disorder in the system, such that one can describe it in terms of a diverging length scale of localization at the transition. This would be given by an exponent ν, such that $L_{\mathrm{loc}} \propto |(g - g_c)/g_c|^{-\nu}$. With the assumption that close to the transition, β can be approximated by a linear function in $\ln g$, this exponent is simply given by the inverse slope of β at the transition. In the framework of scaling theory, no exact value can be given for this exponent, however extrapolating β from its known dependencies at large and small disorder, Abrahams, Anderson, Licciardello and Ramakrishnan (1979) obtain an upper bound of $\nu < 1$. As a matter of fact, John (1984) has shown that expanding the treatment around the lower critical dimension, the exponent should be given by $\nu = 1/2$ in $d = 2 + \epsilon$ dimensions. Such a value for the critical exponent would also be expected for $d > 4$, where it should simply be given by the mean field value of a critical exponent of an order parameter (Schuster, 1978).

At the transition, the loss of transmission can be described by a scale dependence of the diffusion coefficient, such that D becomes smaller as the sample size L increases. As discussed above, this results in $D \propto 1/L$. Such a scale-dependent diffusion coefficient can however also be described in the time domain, where the scale dependence corresponds to a decrease of D with increasing path-length. To quantify this, one has to insert the scale-dependent D into the diffuse spread of the photon

cloud: $\langle r^2 \rangle = Dt$. Since D depends on the length scale as $1/L$, we obtain that $D \propto t^{-1/3}$ at the transition (Berkovits and Kaveh, 1990). For states which are localized, i.e., with an exponential decrease of the transmission, the spread of the photon cloud has to be limited to the length scale of L_{loc}, so that in this case we obtain $D \propto 1/t$. Such a time-dependent diffusion coefficient will constitute the hallmark of Anderson localization, and can also be described by self-consistent theories, which predict the temporal scaling of D(Vollhardt and Wölfle, 1980). These theories have been adapted to a semi-infinite, open medium in order to describe the influence of localization on the coherent backscattering cone by van Tiggelen, Lagendijk and Wiersma (1995). They obtain a rounding of the cone, which experimentally is difficult to distinguish from absorption. Subsequently, Skipetrov and van Tiggelen (2004) and Skipetrov and van Tiggelen (2006) have applied self-consistent theory to open slabs, which are comparable to an experimental situation. Here they indeed find that in time-resolved experiments, a measure of $D(t)$ could be found that can be studied experimentally. We will describe this in detail below.

2. EXPERIMENTS ON COHERENT BACKSCATTERING

As we have seen above, the enhancement of backscattered light is due to the wave nature of light and the time-reversal symmetry (or reciprocity) of wave propagation. As such it is an illustration of the principle behind Anderson localization. Since light does not interact with itself and thus correlation effects can be ruled out, numerous experiments on coherent backscattering of light – and other waves – have studied directly the influence of disorder, polarization and the scattering process on Anderson localization. In this section we will discuss these experiments, starting with the discovery of coherent backscattering and continuing with other influential factors, such as sample thickness and absorption. Then we will discuss the effects of increased disorder on the backscattering cone before discussing experiments on multiple scattering in clouds of cold atoms. There, the nature of the scattering process is of paramount importance and the symmetries responsible for backscattering can be broken due to internal degrees of freedom of the atom involved in the scattering process. Finally we describe some experiments on coherent backscattering using waves other than light, such as acoustic and matter waves.

2.1 Colloidal Suspensions and Turbid Powders

Soon after the prediction by John (1984) and Anderson (1985) that Anderson localization may be observed with light waves, weak localization was observed in the backscattering from colloidal suspensions by van Albada and Lagendijk (1985) as well as by Wolf and Maret (1985). These two groups used slightly different setups to

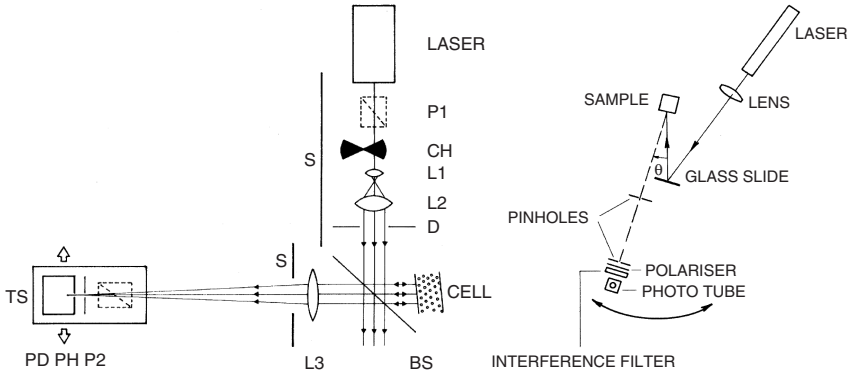

FIGURE 1 The different setups used by van Albada and Lagendijk (1985) (left) and Wolf and Maret (1985) (right) to measure backscattering cones (see text). Reproduced with permission from van Albada and Lagendijk (1985) and Wolf and Maret (1985) © 1985, American Physical Society

study suspensions of polystyrene particles, see Figure 1. van Albada and Lagendijk (1985) illuminated their sample using a beamsplitter, such that the backscattered light can be observed directly using a photomultiplier on a translation stage. In present comparable setups, a CCD camera is used to capture the backscattered light. Wolf and Maret (1985), on the other hand, illuminated the sample using a glass slide as a beamsplitter and placed the detector on a goniometer.

As can be seen from inspection of Figure 2, the two setups obtain very similar results. When the volume fraction of polystyrene particles is increased (thus decreasing l^*), the observed backscattering cone gets wider. Sizeable enhancement factors are found in both cases, but they are still far from the ideal theoretical value of 1. This is due to the fact that the setups lack angular resolution very close to the centre, as well as to a residual effect of direct reflection which is not suppressed completely. These problems were later solved in the setups discussed below.

An enhancement of backscattered light was also found by Tsang and Ishimaru (1984) and Kuga and Ishimaru (1984), however, found the enhancements there were much smaller than those discussed above. Furthermore, both van Albada and Lagendijk (1985), as well as Wolf and Maret (1985) have discussed their findings in the context of weak localization, which was not the case in Kuga and Ishimaru (1984).

Random interference of photons on multiply scattered paths can lead to very large fluctuations in the intensity. These fluctuations are called a speckle pattern. In order to observe a coherent backscattering cone at all, the fluctuations due to the speckle pattern need to be averaged. Using a colloidal suspension, as carried out by van Albada and Lagendijk (1985) and Wolf and Maret (1985), this averaging is achieved by the

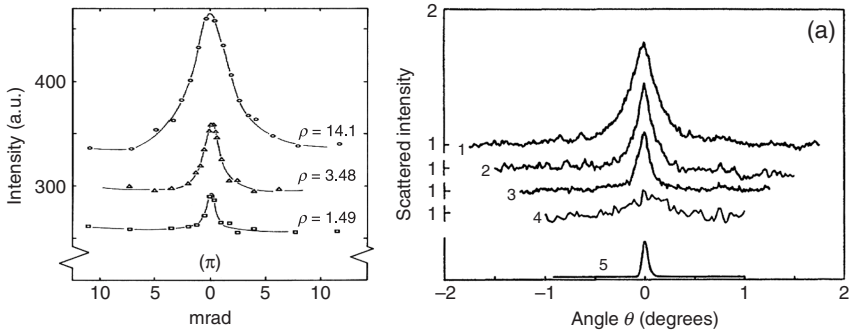

FIGURE 2 The dependence of the backscattering cones on the density of suspended particles (i.e. the mean free path). On the left, the data of van Albada and Lagendijk (1985) are shown with densities varying from 1.4×10^{17} to 1.4×10^{16} m^{-3} and beads of diameter 1.09 μm. On the right, the corresponding data of Wolf and Maret (1985) are shown, where the volume fractions change from 0.004 to 0.11 and beads have diameter 0.49 μm. Due to limited angular resolution, stray light and single backscattering contributions, the enhancements are between 0.4 and 0.6. Reproduced with permission from van Albada and Lagendijk (1985) and Wolf and Maret (1985) © 1985, American Physical Society

motion of the scatterers, which leads to a redistribution of the path-lengths. In fact, studying the decrease of the time autocorrelation of a speckle spot directly gives information of the motion of the scatterers. This was developed into the technique known as diffusing wave spectroscopy by Maret and Wolf (1987) and Pine, Weitz, Chaikin and Herbolzheimer (1998) to extract information on particle size, flow rates and relaxation dynamics in complex turbid fluids. In turbid powders, the averaging over the speckle pattern is usually done by rotating the sample, which leads to a configurational average (see, for instance, Gross, Störzer, Fiebig, Clausen, Maret and Aegerter (2007)).

2.1.1 Experimental Setups for Large Angles

In order to be able to characterize highly turbid samples, in addition to the relatively dilute suspensions discussed above, an apparatus capable of resolving rather large angles is needed. A rough estimate of the angles needed for samples close to the Ioffe–Regel criterion (Ioffe and Regel, 1960) results in a cone width of up to 40°. Even taking into account the narrowing of the cone due to internal reflections at the surface (see below) this means that in order to properly determine the level of the incoherent background, angles up to at least 40° need to be measured. However, at the same time the setups should be able to resolve the cone tip with great accuracy in order to observe deviations from the ideal tip shape (see below). These two requirements pose a big challenge, which has been

solved to some extent (angles up to 25°) by Wiersma, van Albada and Lagendijk (1995) and Gross, Störzer, Fiebig, Clausen, Maret and Aegerter (2007) (angles up to 85°) in two very different ways.

The setup of Wiersma, van Albada and Lagendijk (1995) combines a movable detector with the method of using a beamsplitter to be able to observe the most central angles to high accuracy. Instead of just moving the arm of the detector, an ingenious scheme is used whereby the sample, detector and beamsplitter are moved in concert to ensure that the detected light is always perpendicular to the detector and the incident light is always perpendicular to the sample surface. This is to ensure that the polarizer (P in Figure 3) is always arranged such that direct reflections are extinguished completely. The angular range covered by the setup is, however, limited by the presence of the beamsplitter to below 45°, such that the incoherent background in extremely wide cones cannot be assessed. On the other hand, a single setup can cover all angles up to 25° at almost unlimited resolution with an extinction rate for singly reflected light of nearly 100 per cent.

A radically different approach was chosen by Gross, Störzer, Fiebig, Clausen, Maret and Aegerter (2007). Here, moveable parts are completely absent and the backscattered intensity is measured at all angles simultaneously (Figure 4). This is done via a set of 256 highly sensitive photodiodes placed around an arc of a diameter of 1.2 m. At the very centre of the arc, photodiode-arrays are used that yield a limiting angular resolution of 0.14°. At higher angles the diodes are increasingly far apart, such that at angles $>60°$ the resolution is 3°. In addition, the central 3° of the cone are measured using a beamsplitter and a CCD camera similar to those described above. This gives good overlap with the central part of the wide-angle apparatus, such that effectively the whole angular range is covered, while still measuring the tip of the cone with a resolution of 0.02°. The problems of perpendicular incidence onto the circular polarizers discussed above is solved by using a flexible polarizer foil placed in front of the whole arc. Such a polymer-based polarizer has the disadvantage that only about 96 per cent of the reflected light is extinct, so that enhancements of 2 as obtained by Wiersma, van Albada and Lagendijk (1995) are not possible with this setup. On the other hand, such a polarizer is much cheaper to obtain and can be used in a larger window of wavelengths than a linear polarizer and quarter-wave plate. For wavelength-dependent studies this is a great advantage. Furthermore the renunciation of movable parts makes it possible to measure the small intensities at very large angles with reasonable accuracy.

In addition, very broad backscattering cones pose a problem in that they would seriously breech conservation of energy. As the total reflectivity of an infinitely thick, non-absorbing sample should be $R = 1$, the photon energy within the backscattering cone must be obtained from

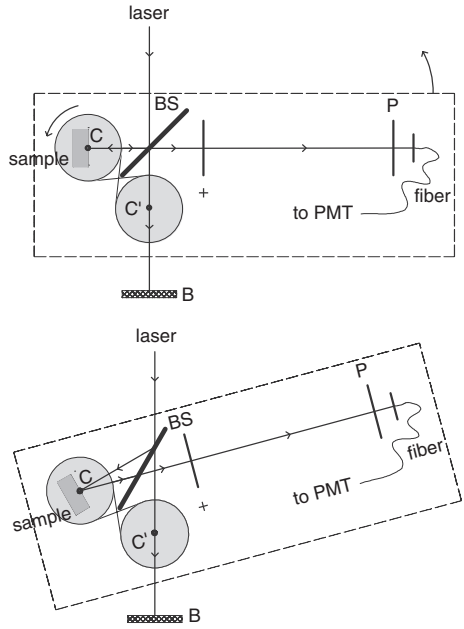

FIGURE 3 The wide-angle setup of Wiersma, van Albada and Lagendijk (1995). The top and bottom panels show the setup at two different angles and illustrate the rotation of the sample, the beamsplitter and the detector are in concert in order to always keep the incident light perpendicular on the sample and the detected light perpendicular on the detector. This is to reduce aberrations in the polarizer when the light is incident at an angle, such that enhancement factors of unity can actually be measured. Reproduced with permission from Wiersma, van Albada and Lagendijk (1995) © 1995, American Physical Society

destructive interference at other scattering angles. In order to be able to tackle this problem experimentally, a calibrated energy scale would be needed. A simple extension of the setup of Gross, Störzer, Fiebig, Clausen, Maret and Aegerter (2007) is capable of this, as will be described below.

2.1.2 Absorption and Finite Thickness

In all of the above, we have assumed that the sample can be treated as in infinite half-space, such that all incident photons are eventually backscattered at the sample surface. In reality, this is not always a good approximation and photons may either be absorbed or leave the sample at the other end or the sides. This implies that the photon path-length distribution needs to be adjusted by suppressing such long paths. This can be done, for instance, by introducing an exponential cut-off to the probability distribution $p(s)$ discussed above, and we expect that the tip of the cone, which corresponds to these long paths, is altered.

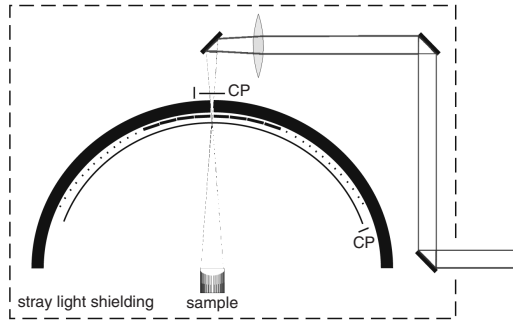

FIGURE 4 The wide-angle setup of Gross (2005). The sample is at the centre of an arc of 1.2 m diameter, which holds 256 sensitive photodiodes. At the centre the diodes are minimally spaced, yielding a resolution of $0.14°$; outwards they are increasingly farther apart up to $85°$. To shield ambient light, the whole setup is placed inside a black box. Direct reflections are suppressed by the use of circular polarization, which is achieved using a flexible polarization foil placed in front of the whole arc. With this, enhancement factors up to 0.96 are possible. The different diodes are calibrated using a teflon sample, which in this angular range gives a purely incoherent signal. Reproduced with permission from Gross, Störzer, Fiebig, Clausen, Maret and Aegerter (2007) © 2007, American Physical Society

van der Mark, van Albada and Lagendijk (1988), Akkermans, Wolf, Maynard and Maret (1988) and Ishimaru and Tsang (1988) have studied this problem quantitatively and find that, indeed, the tip of the cone is rounded. For the simple case of absorption, the cone shape can be obtained by replacing q in equation by $\sqrt{1/L_a^2 + q^2}$(Akkermans, Wolf, Maynard and Maret, 1988), where L_a is the absorption length of the multiple scattering sample, i.e. $\sqrt{l^* l_a/3}$, with l_a the absorption length of the material. This leads to a rounding on the angular scale of $\Delta\theta = 1/kL_a$. The situation is somewhat more complicated for finite samples, but van der Mark, van Albada and Lagendijk (1988) have derived that, in that case, the rounding is on an angular scale of $\Delta\theta = \coth(L/L_a)/kL_a$.

This rounding of the cone has been observed by Wolf, Maret, Akkermans and Maynard (1988) and Schuurmans, Megens, Vanmaekelbergh and Lagendijk (1999), see e.g. Figure 5. Similarly, the scaling of the width of the rounding with sample thickness L and absorption length L_a has been tested experimentally (see Figure 24 below). However, from the discussion above, it is also plausible that localization would lead to a rounding of the backscattering cone since localization too leads to a redistribution of the path-lengths for very long paths. This has been suggested by Berkovits and Kaveh (1987) and calculated using self-consistent theory by van Tiggelen, Lagendijk and Wiersma (1995). We will discuss these issues further in the context of strong localization below.

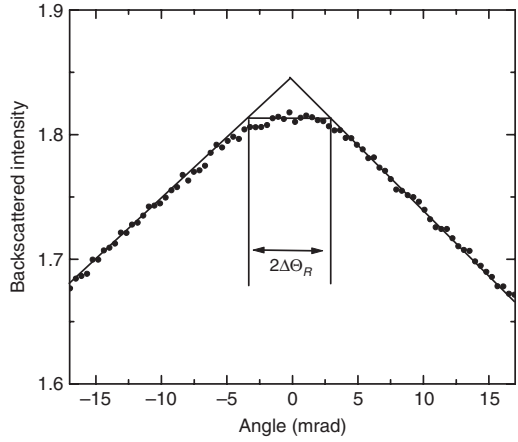

FIGURE 5 Absorption, finite thickness, but also localization of light would lead to a rounding of the cone tip, which ideally would be linear as discussed above. This is because in all of these cases, photons on long paths are not reflected from the sample and therefore do not contribute to the backscattering cone. In these data from Schuurmans, Megens, Vanmaekelbergh and Lagendijk (1999), this rounding can be clearly seen for a sample of photoanodically etched GaP. Due to the lack of an independent determination of the absorption length it is difficult to associate this rounding unambiguously with absorption or localization. Reproduced with permission from Schuurmans, Megens, Vanmaekelbergh and Lagendijk (1999) © 1999, American Physical Society

2.1.3 Surface Reflections

In the above discussion of the shape of the backscattering cone, we have assumed that the cone is directly given by the diffuse path-length distribution of photons at the free sample surface. However, since samples usually have an effective refractive index higher than that of air, this distribution can be influenced by internal reflections of the light as it exits the sample. Such reflections will effectively broaden the path-length distribution, which will lead to a narrowing of the cone. This fact is illustrated in Figure 6. When the path-length distribution broadens, the average distance between the end points of time-reversed paths increases. As is evident within the picture treating the time-reversed paths as double slits, this leads to an increased distance and hence a narrowing of the resulting interference pattern. An averaging over all end-to-end distances then leads to a narrowing of the cone shape. This correction has been calculated quantitatively by Zhu, Pine and Weitz (1991) and Lagendijk, Vreeker and de Vries (1989), who found a strong dependence of the resulting value of kl^* estimated from the full width at half maximum. Instead of FWHM $= 0.75/(kl^*)$ for the scaling of the width as obtained

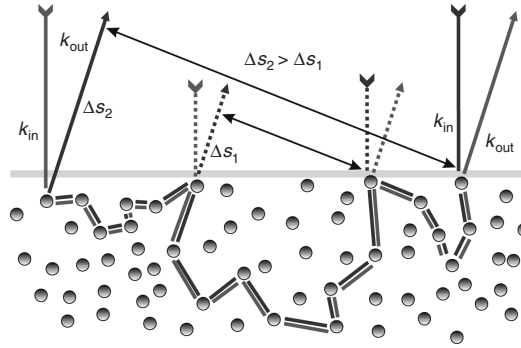

FIGURE 6 If the effective refractive index of the scattering medium is high, internal reflections at the sample boundary may occur. These internal reflections in turn lead to an overpopulation of longer end-to-end distances of photon paths. Since the backscattering cone originates from the interference of time-reversed photon paths, this overpopulation then artificially narrows the measured cones, such that the determination of kl^* directly via the width leads to an overestimation of its inherent value

from Equation (3), Zhu, Pine and Weitz (1991) find a scaling as:

$$\mathrm{FWHM}^{-1} = \left(\frac{2}{3} + \frac{2(1+R)}{3(1-R)}\right) kl^*, \tag{7}$$

where R is the angular averaged reflectivity due to the index mismatch. Thus the values of kl^* obtained from a fit to Equation (3) need to be corrected by a factor of $1/(1-R)$. This correction becomes important in the quest for Anderson localization as in that case the particles are very strongly scattering and the samples therefore have relatively high refractive indices. Thus they show increased internal reflections, which would lead to an overestimation of the value of kl^* solely from the width of the backscattering cone. In order to perform the above correction, the refractive-index mismatch at the surface of the sample needs to be known, i.e. the effective refractive index of the sample needs to be calculated. To a first approximation, this can be done following Garnett (1904), but this approach is strictly valid only for particles with a small refractive index. In order to take into account the strong scattering cross-sections of the particles, more elaborate schemes are necessary. Such calculations have been pioneered by Soukoulis and Datta (1994) and Busch and Soukoulis (1996).

2.1.4 Recurrent Scattering

As the turbidity of the samples increases, there is an increased probability for multiple-scattering paths to return upon themselves. In the extreme

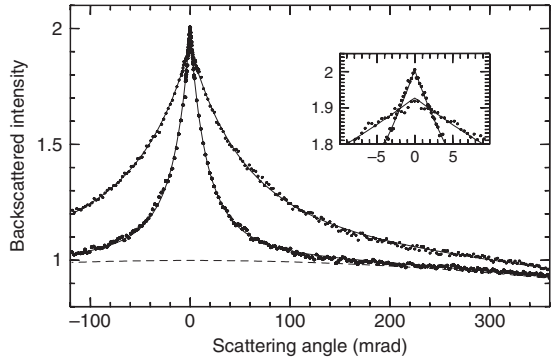

FIGURE 7 For very turbid samples, the enhancement in the backscattering direction is reduced, as can be seen from a close-up at the cone tip of different samples. This is argued to be due to an underpopulation of time-reversed paths because for very turbid samples, there is an increased probability of visiting the same scatterer twice in a multiple-scattering path. Therefore such paths do not contribute fully to the interference pattern resulting in the backscattering cone. Reproduced with permission from Wiersma, van Albada, van Tiggelen and Lagendijk (1995) © 1995, American Physical Society

case, this will lead to Anderson localization, when such paths become macroscopically populated. Wiersma, van Albada, van Tiggelen and Lagendijk (1995) have studied the backscattering cone for increasingly turbid samples and have found that with decreasing kl^*, the enhancement factor of the backscattering cone is reduced. When the first and last scatterer of a multiple-scattering path are the same, the contribution of the interference with the time-reversed path will be the same as that of the background. This implies that the background will be overestimated, leading to a reduction of the enhancement factor. This is illustrated in Figure 7 for two different samples with values of kl^* of 22 and 6, respectively. Due to the high resolution and wide angular range of their setup described above (Wiersma, van Albada and Lagendijk, 1995), the enhancement factor is claimed to be determined to roughly 1 per cent. Thus the reduction shown in Figure 7 should be significant.

It should be noted however that in these measurements of the backscattering cone there is no absolute determination of the intensity scale. The level of the incoherent background is simply determined from a cosine-shaped fit in addition to the backscattering cone described by Equation (3). As such, the backscattering cone would violate the conservation of energy, so that in such strongly scattering samples the absolute intensity needs to be known. This will be discussed in more detail below, where the enhancement is determined over the full angular range with an absolute intensity scale. In fact, the incoherent background can differ by a few per cent as the turbidity changes. For instance, as

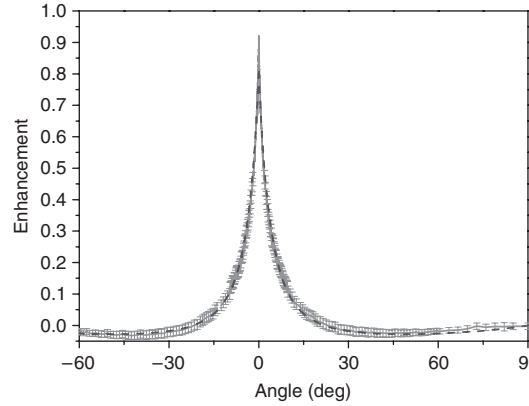

FIGURE 8 A backscattering cone taking into account the absolute intensity scale. Note that there is a negative contribution at high angles balancing the intensity in the cone. This negative part of the enhancement can be described by a correction based on the finite width of the time-reversed paths. Such a corrected theory is shown by the dashed line. Data from Fiebig, Aegerter, Bührer, Störzer, Montambaux, Akkermans and Maret (2007)

the turbidity increases so does the effective size of the sample, such that the albedos of the different samples may no longer be comparable due to losses at the sample boundary. Similarly, the absorption lengths of the different samples will be different, such that the intensity scale may need to be adjusted. This might be the case for the data in Figure 7, where the broad cone is more consistent with a rounded tip, and thus seems to have a somewhat higher absorption than the sample with a perfect two-fold enhancement. As it stands, in the absence of an absolute determination of the incoherent background, the enhancement factor cannot be determined with an accuracy of one per cent. Thus the observed decrease may not be significant.

2.1.5 Energy Conservation

From the discussion so far it would seem that coherent backscattering violates the conservation of energy: In all of the theoretical calculations discussed above (e.g. Akkermans, Wolf and Maynard (1986) and van der Mark, van Albada and Lagendijk (1988)), the enhancement of the cone is always positive irrespective of angle and polarization channel. Thus for a non-absorbing sample covering an infinite half-space (i.e. with a reflectivity of 1), more intensity would be scattered back from the sample than is incident. Obviously this cannot be, and there has to be a correction to the angular intensity distribution at high angles, which compensates for the enhancement in the back-direction. However, this correction is small, and in order to observe it one needs to determine the incoherent

background absolutely. This was not done so far (e.g., Wiersma, van Albada, van Tiggelen and Lagendijk (1995) and Störzer, Gross, Aegerter and Maret (2006)) and the backscattering cones thus obtained were well described by Equation (3). Figure 8 shows the result of such a correction. Here the incoherent reference was a teflon sample, where the absorption was determined using a time-of-flight measurement (Fiebig, Aegerter, Bührer, Störzer, Montambaux, Akkermans and Maret, 2007). Also shown in the figure is a corrected theory, taking into account the fact that time-reversed paths start to overlap when the mean free path gets smaller than the wavelength of light. This leads to an underpopulation on these paths and hence to a reduction of the backscattering enhancement. This is indicated in the sketch in Figure 9, where the overlap of two Gaussian distributed lightpaths is shown. Since this reduction takes place on a length scale of λ, the corresponding reduction of the backscattering enhancement is at high angles. To a first approximation, this correction can be calculated as (Fiebig, Aegerter, Bührer, Störzer, Montambaux, Akkermans and Maret, 2007):

$$\alpha(q) = \frac{3/7}{(1+ql^*)^2}\left(1+\frac{1-\exp(-4/3ql^*)}{ql}\right) - \frac{9\pi}{7(kl^*)^2}\left(\frac{\cos\theta}{\cos\theta+1}\right). \tag{8}$$

The dashed line in Figure 8 is a fit of this equation to the backscattering data with kl^* as the only fit parameter; it is in very good agreement with the data. Furthermore, the integrated intensity over the backscattering half-space of this expression (and of the corresponding data) is nearly zero for all values of kl^*, showing that, by including this correction, energy is indeed conserved for coherent backscattering. This result can also be obtained from diagrammatic theory (Akkermans and Montambaux, 2006). Here it can be shown that the Hikami-box (Hikami, 1981) describing coherent backscattering contains not only the most-crossed diagrams, but also those dressed with an impurity. These diagrams give a contribution of the same order, but negative. It can then be shown exactly that the integral over the whole Hikami-box is exactly zero, which corresponds to the conservation of energy.

2.2 The Influence of a Magnetic Field

As discussed in detail above, coherent backscattering is fundamentally an interference effect due to the wave nature of light. In order to show this experimentally, one needs to change the phase of the light on counterpropagating paths, such that time-reversal symmetry is broken. A possible mechanism for the breaking of time-reversal symmetry is the

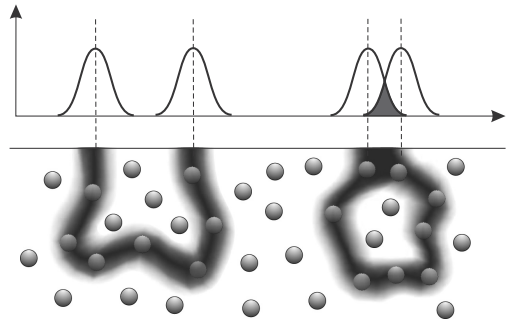

FIGURE 9 Illustration of the physics behind the reduction of the backscattering enhancement. When the mean free path gets shorter, the end points of the multiple scattering paths start to overlap. Describing these as Gaussian distributions with a width λ, one obtains the correction of Equation (8)

application of a magnetic field. As shown by Faraday (1846), an applied magnetic field will change the polarization angle of light passing through a material. This is very pronounced for materials containing paramagnetic rare-earth elements, as they possess absorption bands that lead to a very strong Faraday effect. The magneto-optical rotation of a material is quantified by the Verdet constant, which is the constant of proportionality between the change in phase angle and the applied magnetic field times the length of the light path.

Given the importance of time-reversal symmetry to coherent backscattering and the possibility of influencing the phase of light inside a multiple scattering medium via the Faraday effect, Golubentsev (1984) and MacKintosh and John (1988) have theoretically studied the effect of a medium with a high Verdet constant on the coherent backscattering cone. Due to the fact that we are dealing with a multiple-scattering medium, things are not so simple that it would suffice to project the multiple-scattering path on to the applied field in order to obtain the mean angle of rotation of the phase. In fact, because multiple scattering leads to a depolarization of the light, the average rotation of the phase will be exactly zero irrespective of the applied field and the path-length through the material. However, MacKintosh and John (1988), in a model where every scattering event is assumed to randomly change the polarization of the light, found that the mean square displacement of the phase rotation does follow the Faraday effect. They found that

$$\langle \Delta\alpha^2 \rangle = \frac{4}{3} V^2 B^2 s l_f^*, \tag{9}$$

where s is the length of the path and l_f^* is a length scale describing the depolarization of the photons. This length scale will be of the order of

the mean free path l^*, but will depend on the depolarization properties (and hence sizes) of the scattering particles. We will discuss a numerical investigation of these issues in more detail below. From this result it can be concluded that on path-lengths exceeding $(l_f^*(2VB)^2)^{-1}$, photons on counterpropagating paths can no longer interfere with each other, such that localization is destroyed.

Other effects of magnetic fields on light transport in random media have been discussed as well; these include the existence of the analogue of the Hall effect for photons (Rikken and van Tiggelen, 1996; Sparenberg, Rikken and van Tiggelen, 1997), as well as that of transverse diffusion of light (van Tiggelen, 1995).

2.2.1 Destruction of the Backscattering Cone

As discussed above, for sufficiently strong magnetic fields, Verdet constants and path-lengths, the Faraday effect will lead to a suppression of interference of counterpropagating photons. As we have seen above, the cone tip is due to the longest paths, so that to a first approximation, one could describe the cone in the presence of a magnetic field by introducing the length scale $(l_\mathrm{f}^*(2VB)^2)^{-1}$ as an absorption length in the expression for the cone. With increasing field, this length scale decreases, such that eventually the cone should disappear completely. The field strength at which the cone would be reduced to half its size can be estimated by noting that the width corresponds to a length scale of l^*, so that (taking $l_f^* = 2l^*$ for simplicity) $B = 1/Vl^*$. For a molten Faraday active glass, with a Verdet constant of roughly 10^3 1/Tm and a mean free path of roughly 100 μm, one obtains a field of roughly 10 T. A corresponding experiment was carried out by Erbacher, Lenke and Maret (1993), who studied the field dependence of the backscattering cone in a Faraday-active glass powder in fields up to 23 T. As can be seen in Figure 10, the application of 23 T to the material leads to an almost complete destruction of the backscattering cone, in accordance with the theoretical prediction. For the theoretical curves, q^2 was replaced by $q^2 + q_F^2$, where $q_F = 2VB$ describes the depolarization due to the magnetic field.

2.2.2 Polarization Effects

The simple helicity-flip model of MacKintosh and John (1988) provides a satisfactory description of the data when the incident light is parallel to the applied field. However, if the field is perpendicular to the illumination, the cone shape can no longer be described by a modified version of Equation (3), as was shown by Lenke, Lehner and Maret (2000). In fact, as can be seen in the left-hand panel of Figure 11, the backscattering cone may even split into two peaks, which then diminish in intensity. In order to describe these data, the polarization dependence of the scattering process has to be taken into account, which goes beyond the helicity-flip model

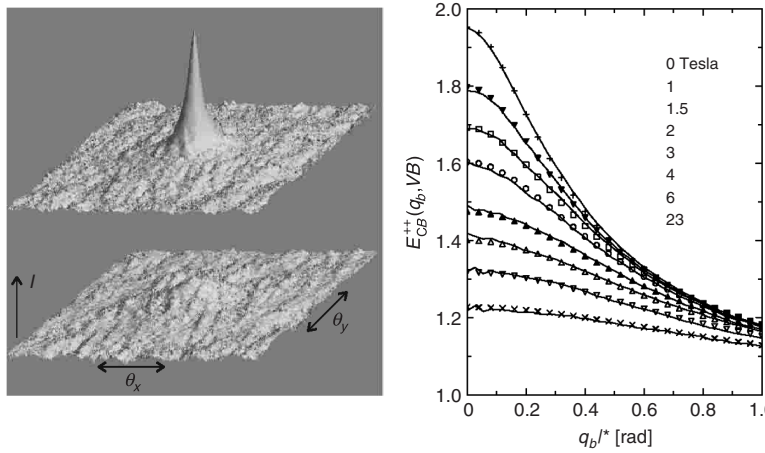

FIGURE 10 Destruction of the backscattering cone by a magnetic field. The left-hand panel illustrates the destruction of the cone in both angular dimensions, while the right-hand panel describes the reduction of the enhancement as a function of different applied fields. The data are from Lenke and Maret (2000)

and has to be done numerically. Such an investigation was carried out by Lenke and Maret (2000). In their treatment, Faraday rotation takes place only between scattering events, as is the case in the helicity-flip model of MacKintosh and John (1988), but at each point in a simulation of a random walk, the full scattering matrix of Rayleigh–Debye–Gans theory is applied to the polarization. The result of such a simulation is shown in the right-hand panel of Figure 11. As can be seen by comparing both parts of the figure, the simulation can qualitatively describe the data. Physically, this splitting of the cone peak is due to the fact that in this transverse setup there is a net, magnetic-field dependent phase change on the time-reversed paths given by the end-to-end distance. This phase difference needs to be compensated for by the phase change due to the path-length difference at different angles. For circular polarization, this leads to a shift of the peak, whereas in linear polarization, the different angular directions are equivalent, such that a splitting of the cone peak is observed (Lenke and Maret, 2000).

In this description, the magnetic-field effects on the backscattering cone are fundamentally determined by the length scale l_f^*, which describes the polarization. For Rayleigh scattering, it can be shown that $l_f^* = 2l^*$(Lenke and Maret, 2000). However, as the scattering particles increase in size, Mie theory has to be used to describe the polarization effects of each scattering event. This has been studied by Lenke, Eisenmann, Reinke and Maret (2002) for different-sized particles of the order of the

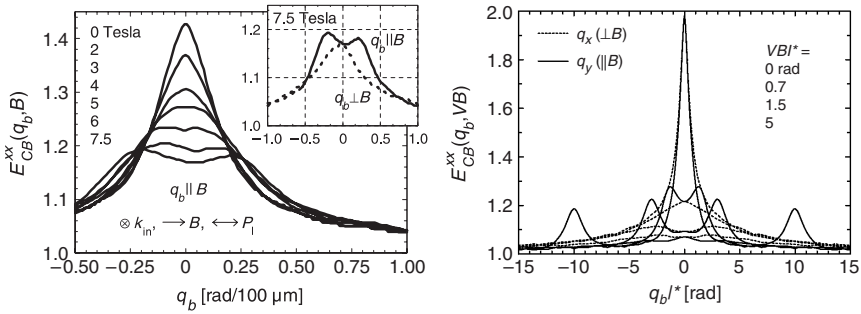

FIGURE 11 The influence of the field direction and the incident polarization on the backscattering cone in a magnetic field. Experimental data are on the left, simulation results on the right. If the field is not applied parallel to the incident light, the destruction of the cone cannot be described by a modified version of Equation (3). However, a simulation taking into account the full scattering matrix for all scattering events on a multiple scattering path can describe the data. Adapted from Lenke and Maret (2000) and Lenke, Lehner and Maret (2000)

wavelength of light, where good agreement is found with the predictions from Mie theory.

2.3 Cold Atoms

With the advent of laser cooling and the corresponding successes in cooling atomic gases to very low temperatures, a new field of investigation of multiple scattering has been opened. Due to the fact that in a cold cloud of atoms all scatterers are identical, one can exploit the properties of resonant scattering in order to increase the scattering cross-section many-fold. In the future this may allow a reduction of kl^* for these samples to such values that the Ioffe–Regel criterion is fulfilled and Anderson localization can be observed. So far however, only the backscattering cone has been observed and the situation has proved to be somewhat more complicated than was hoped at first. This is because of the importance of microscopic degrees of freedom in atomic scattering, which can greatly influence, e.g., time-reversal symmetry. This will be discussed in detail below, and can lead to the observation that the backscattering cone is not destroyed by the presence of a magnetic field as we have seen above, but rather is recovered due to a magnetic field. At present, investigations of multiple scattering of light in cold atomic gases are limited to Rb and Sr, which show vastly different behaviours due to their different ground-state degeneracies.

2.3.1 Rb Atoms

Due to the fact that the cooling of Rb atoms is well known and understood, the first backscattering cones from cold atomic gases were scattered

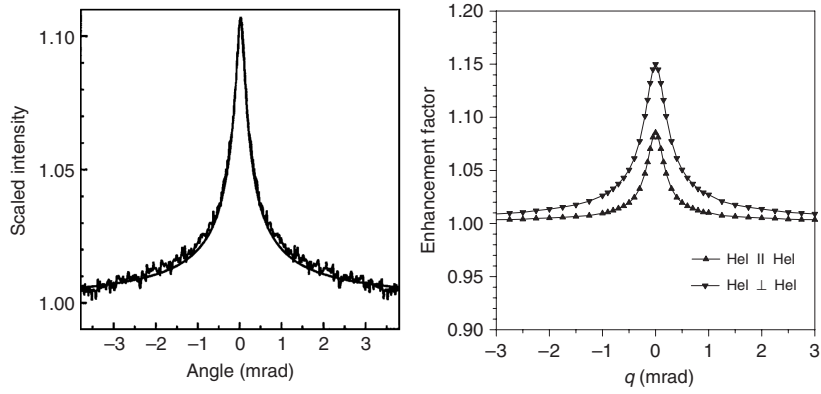

FIGURE 12 Backscattering cone from a cloud of cold Rb atoms (left panel shows data from Labeyrie, de Tomasi, Bernard, Müller, Miniatura and Kaiser (1999), right panel shows data from Kupriyanov, Sokolov, Kulatunga, Sukenik and Havey (2003)). Note that the enhancement factor is very low compared to that seen for colloidal suspensions or powders. This is connected to the internal degrees of freedom of the atoms in question as will be discussed in the text. Reproduced with permission from Labeyrie, de Tomasi, Bernard, Müller, Miniatura and Kaiser (1999) and Kupriyanov, Sokolov, Kulatunga, Sukenik and Havey (2003) © 1999, and 2003 American Physical Society

by Rb atoms (Labeyrie, de Tomasi, Bernard, Müller, Miniatura and Kaiser, 1999; Kupriyanov, Sokolov, Kulatunga, Sukenik and Havey, 2003). However, as can be seen in Figure 12, the observed enhancement is only between 1.1 and 1.15, much smaller that that observed in colloidal suspensions and powders. Due to the internal structure of the Rb atoms, especially the fact that the ground state is degenerate, time-reversal symmetry is partially broken. This is similar to the Faraday rotation effects discussed above for colloidal powders. The degeneracy of the ground state may lead to a change in helicity of the photon during a scattering event, by changing the ground state of the atom (Jonckheere, Müller, Kaiser, Miniatura and Delande, 2000). This could be treated by a model similar to the helicity-flip model (MacKintosh and John, 1988) devised to take into account the effect of Faraday rotation inside a material with high Verdet constant. Müller, Jonckheere, Miniatura and Delande (2001) calculated this explicitly and found good agreement with the experimental reduction of the cone enhancement (Labeyrie, de Tomasi, Bernard, Müller, Miniatura and Kaiser, 1999). They also found that different orders of scattering contribute differently to the effect. In fact, if only double scattering were taken into account, the reduction effect would be much less pronounced, with enhancement factors of up to 1.7 being possible (Jonckheere, Müller, Kaiser, Miniatura and Delande, 2000). By

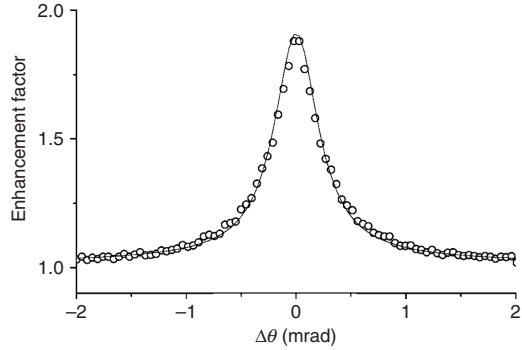

FIGURE 13 Backscattering cone from a cloud of cold Sr atoms (Bidel, Klappauf, Bernard, Delande, Labeyrie, Miniatura, Wilkowski and Kaiser, 2002). Here, almost perfect enhancement is observed due to the fact that the magnetic moment of Sr does not allow for internal degrees of freedom to be scattered from. Reproduced with permission from Bidel, Klappauf, Bernard, Delande, Labeyrie, Miniatura, Wilkowski and Kaiser (2002) © 2002, American Physical Society

lifting this degeneracy using an applied magnetic field, the enhancement of the backscattering cone could be recovered.

2.3.2 Sr Atoms

In order to be able to study a system with a good enhancement factor in the absence of a magnetic field, one needs to use a cloud of atoms with a non-degenerate ground state. This is much more difficult as the cooling transitions are harder to excite in this case. However, using Sr atoms it was possible to cool a cloud sufficiently to observe a coherent backscattering cone (Bidel, Klappauf, Bernard, Delande, Labeyrie, Miniatura, Wilkowski and Kaiser, 2002). The resulting cone is shown in Figure 13 and has an enhancement factor of nearly two in accordance with expectation. Thus the study of Sr clouds may hold the promise of increased coherence length, such that multiple-scattering samples with very long coherent light paths can be studied. This may then lead to the observation of Anderson localization in such samples.

In this context it should be noted, however, that due to the exploitation of resonance scattering to reduce the mean free path, the propagation speed of photons is slowed down remarkably (Labeyrie, Vaujour, Müller, Delande, Miniatura, Wilkowski and Kaiser, 2003). This means that the increased dwell time in the scattering cavity may also lead to a loss of coherence due to the motion of scatterers on this time scale. This was investigated using Monte Carlo simulations by Labeyrie, Delande, Müller, Miniatura and Kaiser (2003), who showed that only a few scattering events are taking place with coherent light, such that the long multiple-scattering paths necessary for Anderson localization to occur are out of

reach. We will get back to the point of reduced transport velocity due to resonant scattering in the discussion of colloidal powders below.

2.4 Other Types of Waves

In addition to localization of light waves and electronic waves, localization has been searched for in many other types of waves. Given the difficulties faced by electron localization due to the presence of interactions, these studies have focused on non-interacting waves, such as acoustic, seismic and matter waves. Due to the fact that strong scattering cross-sections are difficult to obtain in these waves, most studies have concentrated on the observation of weak localization.

2.4.1 Seismic Waves

Multiple scattering of seismic waves has become a very interesting subject, leading, for instance, to an increased precision in the determination of the earth's structure from the noise in seismographs (Snieder, Grêt, Douma and Scales, 2002; Campillo and Paul, 2003; Shapiro, Campillo, Stehly and Ritzwoller, 2005). In the context of interest here, Larose, Margerin, van Tiggelen and Campillo (2004) have studied the reflection of a stimulus from a sledge hammer that was repeated fifty times for each measurement as a function of distance from the source. The results are shown in Figure 14. The different lines correspond to different delay times between the stimulus and the reflected signal. As expected from the theoretical description above, the backscattering cone arises from long multiple-scattering paths, such that the signal only appears at long delay times. In particular, as can be seen in the figure, an enhancement factor of two can be observed from the long paths observed at late times.

In order to be able to observe this enhancement, i.e. to suppress any incoherent background, the experiment was carried out at night in a sparsely populated region as well as under anticyclonic conditions.

2.4.2 Acoustic Waves

Well before the study of seismic waves propagating in disordered media, the behaviour of multiple scattered ultrasonic waves in the MHz range was investigated. Kirkpatrick (1985) has theoretically calculated the properties of localized waves in a random medium, and Bayer and Niederdränk (1993) have experimentally studied the backscattering cone from, e.g., gravel, using ultrasonic waves. This was done in both two- and three-dimensional systems and good agreement with theory was found, as illustrated in Figure 15.

There have also been experiments studying time-resolved transmission of acoustic waves through samples of aluminium beads by Page (Page, J.H. (2007) private communication). In these experiments, a non-exponential decay of the time-resolved transmission was found. As will

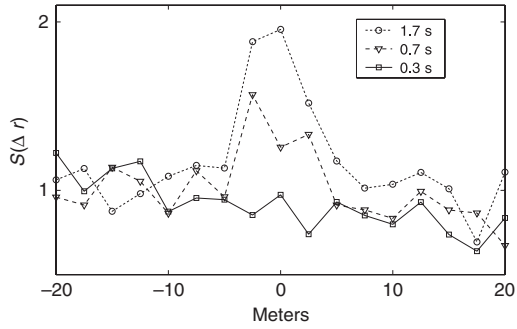

FIGURE 14 Backscattering cone of seismic waves produced by Larose, Margerin, van Tiggelen and Campillo (2004). The different lines show the signal of buried seismographs at a certain distance from the stimulus as a function of delay time. After prolonged times, the multiply scattered paths in the back-direction show a coherent backscattering cone with an enhancement factor of nearly 2. Reproduced with permission from Larose, Margerin, van Tiggelen and Campillo (2004) © 2004, American Physical Society

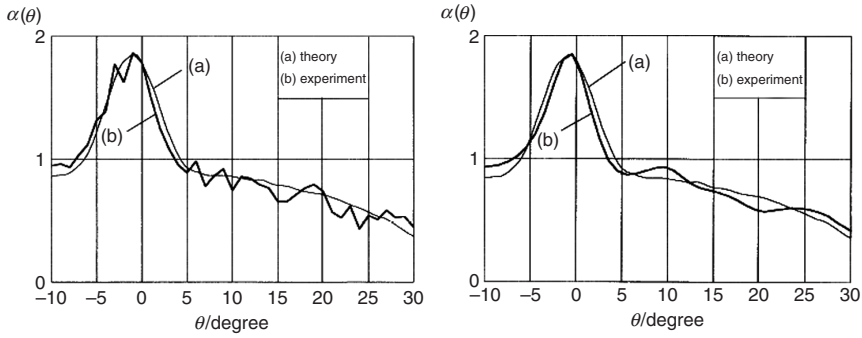

FIGURE 15 Backscattering cone of ultrasonic waves through (left) gravel stones and (right) brass rods. These data were obtained by Bayer and Niederdränk (1993). The thin lines show the theoretical expectation (Kirkpatrick, 1985), whereas the thick lines show the experimental results. The data correspond to signals at a certain time delay, similar to those of the seismic waves in Figure 14 of 22 μs and 40 μs, respectively. Reproduced with permission from Bayer and Niederdränk (1993) © 1993, American Physical Society

be discussed below in the context of light, this is a strong indication of non-classical transport and localization. In addition, Page (Page, J.H. (2007) private communication) studied the statistics of speckles for these samples, and again found strong deviations from the behaviour of diffuse waves.

2.4.3 Matter Waves

Two different types of matter waves are presently the subject of localization efforts. In the first instance, the advent of laser cooling and optical traps has led to the proposal of studying Anderson localization of cold atoms in disordered optical traps. These optical traps are usually provided by a speckle pattern from a laser source passed through a disordered medium. It has been found however that in that case, the average spacing of the speckle spots is difficult to reduce to a scale where the Ioffe–Regel criterion can be reached (Lye, Fallani, Modugno, Wiersma, Fort and Inguscio, 2005; Clément, Varón, Hugbart, Retter, Bouyer, Sanchez-Palencia, Gangardt, Shlyapnikov and Aspect, 2005; Kuhn, Miniatura, Delande, Sigwarth and Müller, 2005). In addition, dense clouds of cold atoms are troubled by strong interactions, such that a Mott insulator can be observed, but Anderson localization is still out of reach in present experiments. In fact, no observation of a backscattering cone of cold atoms in disordered optical lattices has been reported to date.

A second type of proposal is to localize ultracold neutrons in the presence of disorder (Igarashi, 1987). Here, progress has been made in cooling the neutrons sufficiently to be able to observe their multiple scattering. The angular resolution of neutron detectors is, however, not sufficient at present to observe the corresponding, narrow backscattering cone (Stellmach, Abele, Boucher, Dubbers, Schmidt and Geltenbort, 2000; Stellmach, 1998).

3. THE TRANSITION TO STRONG LOCALIZATION

In the experiments described above, the critical parameter for localization, the disorder as measured by $(kl^*)^{-1}$, was small compared to unity. However, the effects of weak localization could still be observed as there is a counterpropagating path to every path in the back-direction. In order to see the effects of strong localization, one needs to strongly increase the probability of formation of closed loops, so that the renormalization discussed in the theory part becomes important. This can be done in principle by increasing the disorder so as to reach the limit proposed by Ioffe and Regel (1960). In practice however, this turns out to be difficult as one needs to have samples with both strong scattering and low absorption, two conditions which are usually mutually exclusive. However, it can be accomplished by making use of the properties of Mie-resonances in the scattering cross-section (Mie, 1908), as we will see below. On the other hand, spatially restricting the propagation will lead to a strong increase in the probability of observing crossings of the paths. This is exploited in the study of quasi-one-dimensional systems where localization of microwaves has been observed (see, e.g., Chabanov, Stoytchev and Genack (2000)).

3.1 Low-dimensional Systems

Low-dimensional systems present several advantages for studying localization. First of all, scaling theory predicts that in less than two dimensions, localization will always be present (Abrahams, Anderson, Licciardello and Ramakrishnan, 1979). The occurrence of localization will in this case go together with the increase in system size, and localization effects can be observed for large enough samples. The spatial restriction in quasi-one-dimensional samples leads to a natural reduction of the dimensionless conductance, thus leading to the presence of localization even far above the turbidity demanded by Ioffe and Regel (1960). This, in turn, also implies that the transition to localization cannot be studied in low-dimensional systems, and a proper study of the scaling theory of localization requires three-dimensional systems.

The most successful experimental low-dimensional system so far constitutes a quasi-one-dimensional case, where alumina spheres with a diameter of roughly a centimeter are placed inside a copper tube with a diameter of 7 cm and a length of roughly one meter (Chabanov and Genack, 2001). The alumina particles then scatter microwaves, which are contained in the copper tube as in a wave guide, thus producing the quasi-one-dimensional character of the system.

3.1.1 Statistical Features

The transmitted microwave intensity through the cavity shows strong fluctuations as a function of input frequency (see Figure 16a). Such fluctuations always arise in the case of a multiple-scattering sample. They arise from interferences of the randomly distributed field and are known as speckle. Due to the fact that speckle originates from a random distribution of fields it is easy to show that a diffusive speckle shows an exponential intensity distribution. As can be seen in Figure 16b, in the case of a quasi-one-dimensional sample longer than the localization length, the intensity distribution of the fluctuations is much wider than the exponential distribution expected for a diffusive speckle indicated by the dashed line (Chabanov, Stoytchev and Genack, 2000). The intensity distribution is instead given by a stretched exponential with an exponent of 1/3 (Chabanov, Zhang and Genack, 2003), in agreement with the prediction of Kogan, Kaveh, Baumgartner and Berkovits (1993), whereas Nieuwenhuizen and van Rossum (1995) have predicted a stretched exponential with an exponent of 1/2. This result was later confirmed by Kogan and Kaveh (1995).

The advantage of studying the fluctuations of the intensity rather than the static intensity is that this measure is not affected by the presence of absorption. As we will see in the discussion of static transmission measurements in three-dimensional samples, the presence of absorption can be a great problem in identifying localization from transmission

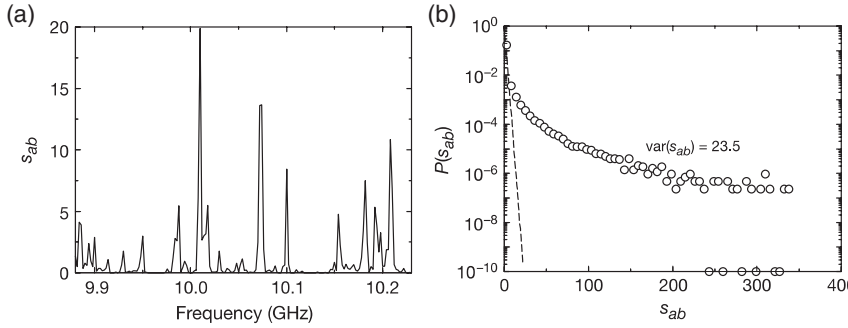

FIGURE 16 Measurements of the fluctuations of photons in a quasi-one-dimensional sample of alumina spheres obtained by Chabanov, Zhang and Genack (2003). (a) The intensity as a function of input frequency for a certain realization of the disorder in the tube. (b) Averaging over many realizations of the disorder, the intensity probability distribution is obtained. This shows clear deviations from the classical exponential distribution and instead shows a stretched exponential with an exponent of 1/3 (Chabanov, Zhang and Genack, 2003). Reproduced with permission from Chabanov, Zhang and Genack (2003) © 2001, American Physical Society

measurements alone. In addition to the probability distribution of the speckle intensities, Sebbah, Hu, Klosner and Genack (2006) have measured the spatial distribution of the localized modes.

3.1.2 The Path-Length Distribution

Another strategy for avoiding problems with absorption influencing the interpretation of experimental results is to study time-resolved transmission. This will be discussed in more detail below in the context of three dimensional systems, but time-resolved measurements were also carried out in the quasi-one-dimensional system described above by Chabanov and Genack (2001). The results of such measurements are shown for four different samples in Figure 17. The samples differ in tube length, ranging from 61 cm (sample A) to 183 cm (sample C). Samples B and D are both 90 cm long but in sample D the absorption was artificially enhanced by adding a titanium foil to the tube.

The data in Figure 17 are shown on a semi-logarithmic scale and show a slight deviation from the purely exponential decrease at long times expected from diffusion. This is shown more clearly in the lower part of the figure, which shows the derivative of the logarithm of the intensity with respect to time. At long times, this should be a constant given by a combination of the absorption length and the diffusion coefficient. As can be seen, the diffusion coefficient instead decreases with time, which is most prominent for sample A. In addition, comparison of samples B and D shows that indeed a change in absorption only leads to a constant shift

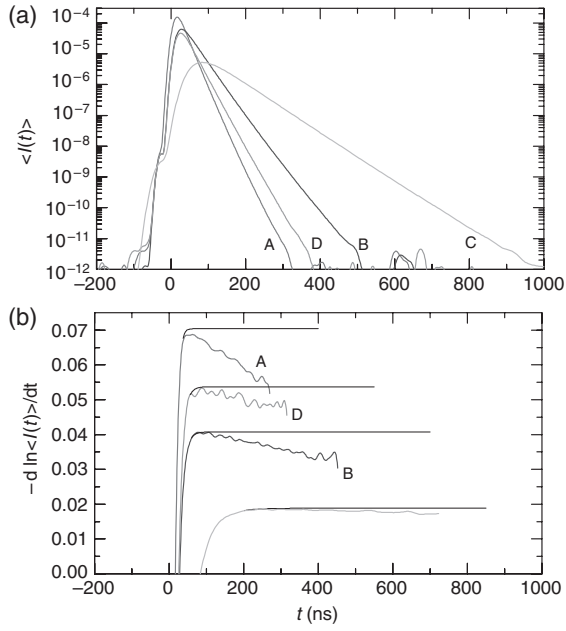

FIGURE 17 Measurements of the path-length distribution of photons in a quasi-one-dimensional sample of alumina spheres of different lengths as obtained by Chabanov and Genack (2001). As can be seen from the lower part of the figure, the diffusion coefficient in these samples shows a time dependence indicating a breakdown of diffusion due to the presence of pre-localized states. Reproduced with permission from Chabanov and Genack (2001) © 2001, American Physical Society

in the decay rate and thus does not influence the results of the time dependence shown in the figure.

In contrast to the results in three dimensions to be discussed below, the diffusion coefficient here decreases linearly with time. This decrease is obtained from weak localization corrections in the quasi-one-dimensional case as discussed by Cheung, Zhang, Zhang, Chabanov and Genack (2004) and Skipetrov and van Tiggelen (2004).

3.1.3 The Connection to Bulk Experiments

As mentioned above, experiments in quasi-one-dimensional systems exploit the increased probability of paths crossing due to the constricted geometry. As a matter of fact, a similar approach was used by Scheffold, Härtl, Maret and Matijević (1997) and Scheffold and Maret (1998) to study the universal conductance fluctuations of light, which are suppressed by a factor of $1/g^2$ compared to the usual fluctuations. These experiments were carried out in a colloidal suspension of TiO_2 particles with values of kl^* of the order of 20. This shows that a geometric confinement gives

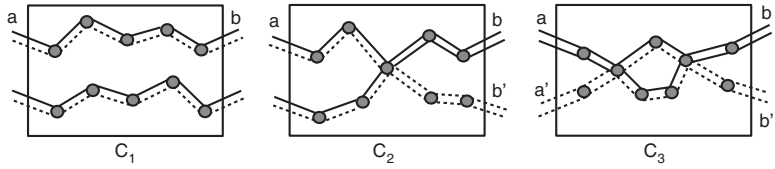

FIGURE 18 The number of diffusive modes is inverse to the probability of crossings of paths inside the sample. For very constrained samples, such as in the case of the quasi-one-dimensional microwave experiments or the measurements on universal conductance fluctuations, the probability of crossings is high and thus the number of modes, i.e. the control parameter for localization, is low. Adapted with permission from Scheffold and Maret (1998) © 1999, American Physical Society

rise to mesoscopic effects (Figure 18); these are similar to the bulk effects of Anderson localization in that they depend on interference between different paths, but they are due solely to geometric effects and thus should not be confused with bulk Anderson localization.

In fact, when estimating the dimensionless conductance (Scheffold and Maret, 1998) for a true bulk sample with dimensions of roughly $10^4\, l^*$, one finds that g is very large. For the samples with very low values of kl^* discussed below, one obtains $g \approx 10^4$(Aegerter, Störzer and Maret, in press). This demonstrates that in bulk samples, the critical parameter is indeed kl^* as opposed to g, and one cannot think of the problem in terms of separated modes. This difference also clearly shows up in the self-consistent theory of Skipetrov and van Tiggelen (2004) adjusted for finite systems. In the quasi-one-dimensional case (Skipetrov and van Tiggelen, 2004) there are pre-localized states and a cross-over to localization, whereas in the three-dimensional version of the theory (Skipetrov and van Tiggelen, 2006) there are no pre-localized states and diffusion only breaks down at later times.

3.2 Static Measurements

Static measurements have the strong advantage experimentally of being reasonably simple to set up. However, in terms of observing localization, there is a great problem with most static measurements insofar as a photon that is lost due to absorption cannot be distinguished from one lost due to localization. Thus, pure measurements of numbers of photons either in transmission or reflection are difficult to interpret in the context of localization. One way around this will be discussed at the end of this chapter; it consists of studying the fluctuations of the static intensity (i.e. the speckle). There, the interference terms are of great importance, so that one does not simply look at numbers of photons, and the effects of localization and absorption can be distinguished (Chabanov,

Stoytchev and Genack, 2000). Another possibility is offered by time-resolved measurements, which will be discussed in the next subsection.

3.2.1 Decrease in Transmission

As discussed above, localization will lead to a strong decrease in the transmission of photons through the sample. In fact, due to the renormalization of the diffusion coefficient, the dependence of the transmission on the sample thickness can be predicted. In the critical regime, where there is no length scale in the diffusion left, scaling theory predicts that the diffusion coefficient will decrease as $1/L$(Abrahams, Anderson, Licciardello and Ramakrishnan, 1979). This leads to a decrease in transmission proportional to $1/L^2$(Anderson, 1985; John, 1984). Deep in the localized regime, where the diffusion coefficient vanishes, the transmission will be suppressed exponentially, as only the tails of the probability distribution are capable of leaving the sample at the boundary (Anderson, 1985; John, 1984). These predictions have been at the basis of an experimental search for localization using static transmission measurements of strongly scattering samples (Wiersma, Bartolini, Lagendijk and Righini, 1997). In this work, the transmission properties of ground samples of GaAs were studied in the near infrared, at a wavelength of 1064 nm. For different degrees of grounding and hence different average particle sizes, marked differences in the thickness dependence of transmission were observed. The scattering properties of the samples were characterized using the initial slope of the coherent backscattering cone, yielding a value of kl^*.

The results for a sample consisting of particles with an average diameter of 1 μm are reproduced in Figure 19. As can be seen in the figure, there are deviations from the expected $1/L$ behaviour corresponding to diffusion. The theoretical prediction shown by the dashed line however, is in strong contradiction with a simple understanding of localization. As shown in the figure, the deviations from classical transmission due to localization lead to an *increase* in static transmission, which is physically impossible. Moreover, the deviations increase with decreasing sample thickness, again in contradiction with a physical understanding of the situation. The theoretical prediction of classical diffusion was obtained from the measurement of kl^* due to the initial slope of the backscattering cone. This yields a mean free path of 0.17 μm and a corresponding value of $kl^* = 1$. The transmission measurements from thin samples are, however, more consistent with a value of $kl^* \approx 5$. In this case the deviations in thicker samples are such that the number of transmitted photons decreases compared to the classical expectation. This implies that the determination of kl^* from the initial slope of the backscattering cone is systematically flawed and underestimates the value of kl^*. As we have seen above, absorption can lead to a rounding of the cone tip. Such a rounding

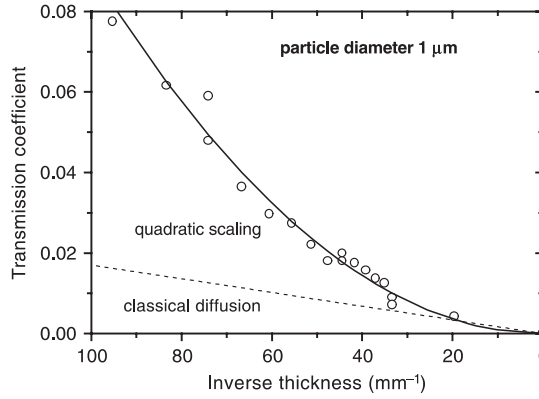

FIGURE 19 Static transmission through samples of GaAs of average particle size $\sim 1\ \mu\text{m}$(Wiersma, Bartolini, Lagendijk and Righini, 1997). As can be seen, the thickness dependence of the transmission does not follow a $1/L$ dependence. However, the dashed line in the figure indicating classical diffusion is inconsistent with a physical interpretation of the data. Any physical effect, be it localization or absorption, would lead to decreased transmission as compared to the classical expectation, whereas the dashed line in fact indicates an *increased* transmission with respect to the diffusive expectation. This is most probably due to the fact that the value of kl^* is underestimated due to neglect of absorption in the sample (see text and Figure 20)

strongly influences the initial slope of the cone, while leaving the width more or less unchanged. Thus the presence of absorption may very well lead to an underestimation of kl^* from the initial slope of the backscattering cone, whereas an estimate from the width of the cone is less susceptible to absorption. This is corroborated by the fact that the value of kl^* estimated above is in good agreement with a re-analysis of the cone shape using the width of the cone to determine kl^* and including absorption, shown in Figure 20(Scheffold, Lenke, Tweer and Maret, 1999).

This re-analysis also leads to an estimation of the absorption length of $L_a \approx 8\ \mu\text{m}$, which is consistent with the transmission data, again shown in Figure 20. This means that the deviations from diffusive behaviour are most probably due to an increased absorption induced by the longer grinding. Such absorption may for instance be due to the increased appearance of surface states.

For even smaller particle sizes (average diameter 300 nm), Wiersma, Bartolini, Lagendijk and Righini (1997) obtain an exponential decrease of transmission with a typical length scale of $L \approx 5\ \mu\text{m}$. Supposing, in the absence of absorption, that with decreasing particle size the mean free path also decreases, this would be in accordance with the prediction of Anderson localization in the localized regime (Anderson, 1985; John, 1984). Unfortunately however, the scattering properties of this sample were not characterized by any measurement, so we do not

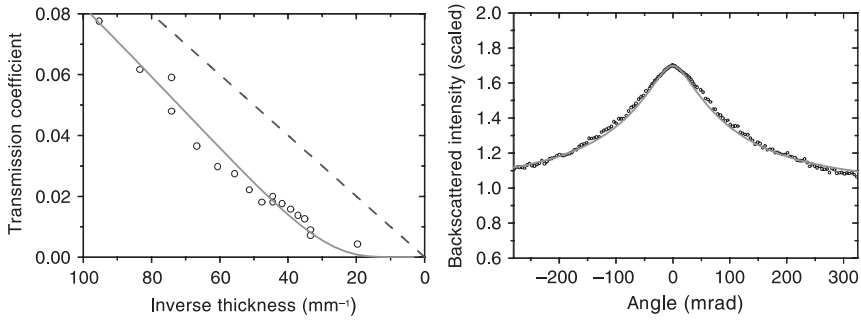

FIGURE 20 The data of Wiersma, Bartolini, Lagendijk and Righini (1997) (see Figure 19) as re-analysed by Scheffold, Lenke, Tweer and Maret (1999). In this analysis, the influence of absorption has been taken into account as well. Thus, the tip of the cone is rounded and the slope at that point cannot be used for a reliable estimate of kl^*. The analysis of the cone shape (right-hand side) yields a value of $kl^* \approx 5$ and an absorption length of $L_a \approx 8\ \mu\text{m}$, which fits the data very well. Using these parameters, the static transmission measurements on the left-hand side can be described without additional parameters. The inclusion of absorption yields the solid line, whereas the classical expectation is given by the dashed line. Note that in contrast to Figure 19, the expectation for pure diffusion is above the data, as it should be

know what the value of kl^* for this sample should be. This also makes it impossible to estimate the absorption length of this sample. Based on the above arguments, absorption will be present also in this sample and the corresponding absorption length would not be inconsistent with the length scale of the exponential decrease in transmission. Furthermore, the decrease in kl^* with particle size is certainly not linear and will certainly show a minimum as the scattering cross-section decreases when the particle size is much smaller than the wavelength of light. Therefore it is questionable whether or not the scattering strength of this sample will be strong enough to be beyond the Ioffe–Regel criterion. In addition, in the absence of an independent determination of the absorption length, an exponential decrease of transmission cannot be claimed to be due to localization, as absorption is a much more likely candidate.

This is illustrated in Figure 21, which shows the static transmission through a sample with $kl^* \approx 20$(Aegerter, Störzer and Maret, in press). For very thick samples, absorption will always dominate and a simple comparison with the expectation from diffusion (dotted line) will always overestimate the transmission. However, in this case, the absorption length was determined directly as well, using time-resolved measurements (see below). Adding this to the description yields the dashed line, which perfectly describes the data without a single adjustable parameter. Here the shaded area between the dashed lines indicates the error bar in the experimental determination of the absorption length.

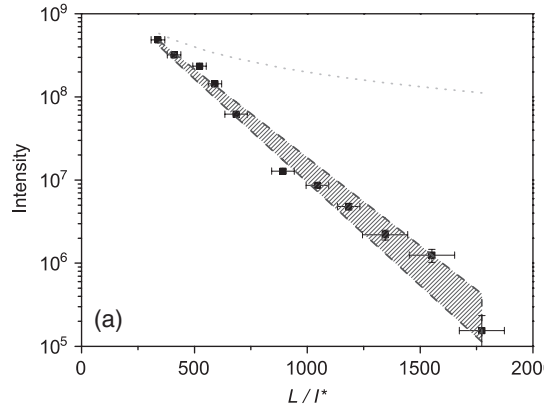

FIGURE 21 Even for a classical sample (with $kl^* \approx 20$) that appears white and which does not show significant rounding of the backscattering cone, absorption may be high enough to produce an exponential decrease in transmitted intensity, which appears incompatible with classical diffusion of light (dotted line) (Aegerter, Störzer and Maret, in press). When determining the absorption length using time-resolved measurements (see below), the resulting exponential decrease (dashed line) fits very well with the static measurements

For samples with much lower values of $kl^* \approx 2.5$, which also show effects of localization in time-resolved measurements (i.e. a spatially dependent diffusion coefficient, see below) the situation is markedly different (Aegerter, Störzer and Maret, 2006). This is shown in Figure 22. Again the dotted line, corresponding to diffusion in the absence of absorption, strongly overestimates the transmission through the samples. However, the description including the experimentally determined absorption (dashed line) is in contradiction with the data as well. Thus in this case the reduced transmission is most probably due to localization of photons. This conclusion is strongly supported by the fact that the time-resolved measurements also allow a determination of the localization length (see below). Including this in the description of the transmission measurements yields the solid line, which describes the data perfectly over twelve orders of magnitude and without any adjustable parameters.

This shows that in static transmission measurements, the problem of absorption may be circumvented by an independent determination of the absorption length. This is most conveniently done in time-resolved measurements as we will discuss below.

3.2.2 Influence on the Cone Shape

As discussed above, the renormalization of the diffusion coefficient arising from localization can also be treated as a path-length dependence of D(van Tiggelen, Lagendijk and Wiersma, 1995). Since the tip

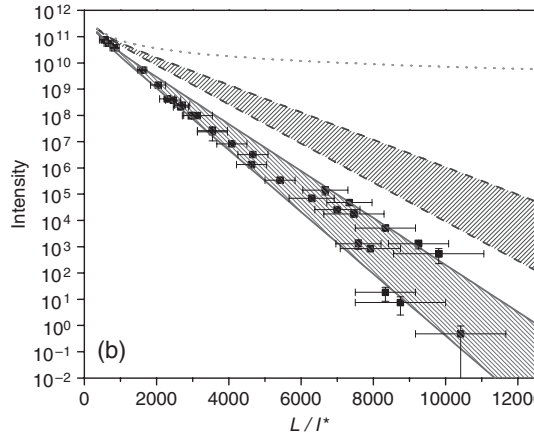

FIGURE 22 Static transmission measurements through a localizing sample as shown by a long-time tail in time-resolved transmission (Aegerter, Störzer and Maret, 2006). As will be shown below, in this case it is possible to determine not only the absorption length, but also the localization length. Again, the dotted line represents the expectation from pure diffusion and the dashed line that of diffusion including absorption. Both curves are incompatible with the measurements, and satisfactory description of the data becomes possible only upon incorporating the experimentally determined localization length. In fact, there is good agreement between theory and experiment over twelve orders of magnitude without any adjustable parameters

of the backscattering cone consists mostly of photons from long paths, such a path-length dependence of the diffusion coefficient should also be visible in the tip of the cone, as a decrease of the slope as the tip is approached. This effect has been calculated explicitly in the framework of self-consistent theory by van Tiggelen, Lagendijk and Wiersma (1995). Their main result is shown in Figure 23, where the decrease of the diffusion coefficient inside the sample is shown together with the corresponding rounding of the cone tip. As discussed above, however, absorption also leads to a rounding of the cone at small angles due to the lack of photons coming from very long paths. Unfortunately, van Tiggelen, Lagendijk and Wiersma (1995) obtain a diffusion coefficient which decreases exponentially with sample thickness (analogous to the exponentially decreasing transmission), so that the effect of localization again has the same shape as that of absorption. This means that, as in the case of static transmission measurements discussed above, measurements of cone-rounding can only be used as arguments for the observation of localization in the presence of data on the absorption properties of the samples.

Indeed, as a function of sample thickness, Schuurmans, Megens, Vanmaekelbergh and Lagendijk (1999) find an increasing rounding of the cone when the thickness is decreased, as demanded by theory (van der

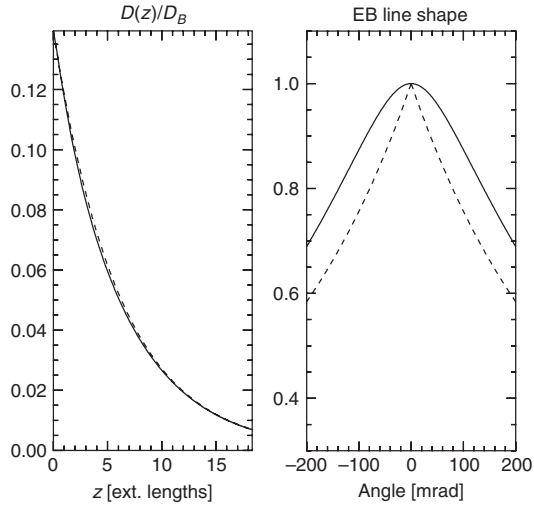

FIGURE 23 The influence of localization on the tip of the backscattering cone. Due to the fact that photons on long paths are localized and therefore no longer contribute to the backscattered light, the cone shape is rounded close to the backscattering directon. Plotted here are results from a self-consistent theory assuming a spatially dependent diffusion coefficient calculated by van Tiggelen, Lagendijk and Wiersma (1995). The left-hand panel shows the spatial dependence of the diffusion coefficient, while the right-hand panel gives the corresponding tip of the backscattering cone. The dashed line on the right is the classical cone shape in the absence of localization effects. Reproduced with permission from van Tiggelen, Lagendijk and Wiersma (1995) © 2000, American Physical Society

Mark, van Albada and Lagendijk, 1988). Samples with reasonably high kl^* (shown as solid triangles and open squares in Figure 24) are well described by the linear increase of the cone-rounding with $1/kL$. For samples with smaller values of kl^* however, there are marked deviations for thicker samples. In order to determine the influence of absorption, Schuurmans, Megens, Vanmaekelbergh and Lagendijk (1999) filled the photoanodically etched GaAs sample with dodecanol, showing increased cone-rounding (see Figure 5). This leads to an increase in kl^* as can be seen from a decrease in the width of the backscattering cone (see Figure 25). Hence the absorption length is also increased according to $L_a \propto \sqrt{l^* l_a}$. A description of the dependence of the cone-rounding on sample thickness of the non-filled sample due to absorption (dashed line in Figure 24) is not compatible with the thickness dependence of the cone-rounding of the filled sample. However, one has to note that in this calculation, Schuurmans, Megens, Vanmaekelbergh and Lagendijk (1999) did not take into account the narrowing of the cone due to internal reflections. The filling of the etched holes will lead to a change in the effective refractive index and hence to

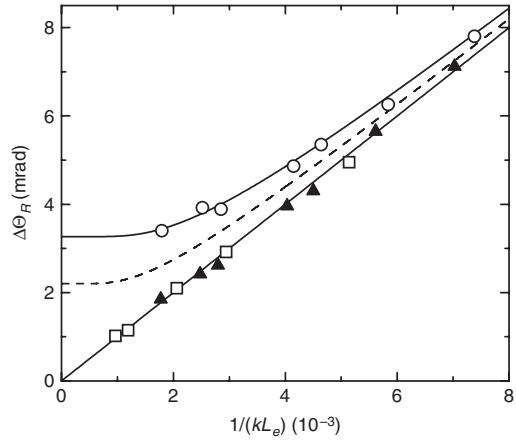

FIGURE 24 The rounding of the cone shown in Figure 5 as a function of sample thickness for different samples (Schuurmans, Megens, Vanmaekelbergh and Lagendijk, 1999). For low values of kl^* (open circles), there are deviations from the expectation of a finite sample. This is in contrast to samples with a higher kl^* (solid triangles and open squares). The open squares are from a similar sample to the open circles, where the pores have been filled with dodecanol. The solid line is a description of the data with absorption. Assuming an unchanged absorption with pore-filling, the dashed line should then correspond to the open squares. Reproduced with permission from Schuurmans, Megens, Vanmaekelbergh and Lagendijk (1999) © 1999, American Physical Society

a change in the value of kl^* determined from the cone width. Thus the filling of the voids may well lead to a decrease in the refractive index and hence to an underestimation in the increase in kl^*. Due to these uncertainties a direct determination of the absorption length in the low-kl^* samples would have been very useful in order to check whether effects of absorption can be ruled out. In addition, subsequent time-resolved experiments on the same samples by Rivas, Sprik, Lagendijk, Noordam and Rella (2000) and Johnson, Imhof, Bret, Rivas and Lagendijk (2003) did not show effects of localization in the time domain. While this could be due to the fact that the time-resolved measurements were done on thinner samples (see also below), we note that the transmission data of Johnson, Imhof, Bret, Rivas and Lagendijk (2003) can be described with an absorption length corresponding to the solid line in Figure 24. It therefore would seem that the increased cone-rounding observed in these samples cannot be used as an indication of the onset of Anderson localization as long as absorption is not quantified.

3.2.3 Transport Speed

Another quantity that can be determined from static measurements is the transport speed of photons in multiple scattering. Since the strong

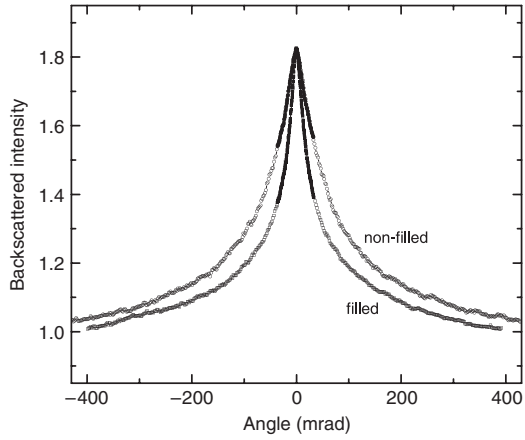

FIGURE 25 The backscattering cones for photoanodically etched GaP both as produced and filled with dodecanol (Schuurmans, Megens, Vanmaekelbergh and Lagendijk, 1999). As can be seen, the cone of the filled material is narrower, indicating an increase in kl^*. Figure 24 has shown that for the filled samples, significantly less cone-rounding has been observed. Reproduced with permission from Schuurmans, Megens, Vanmaekelbergh and Lagendijk (1999) © 1999, American Physical Society

scatterers employed in the search for Anderson localization are roughly of the same size as the wavelength to increase the scattering cross-section, these particles also show resonant scattering (Wigner, 1955). This was first discussed by van Albada, van Tiggelen, Lagendijk and Tip (1991) in the context of multiple scattering. Contrary to what might be thought intuitively, the resonant scattering properties are still present after averaging over the random distribution of scatterers in multiple scattering. This leads to a strong decrease in the transport speed of photons, as can be seen in Figure 26, where the speed of light is shown as a function of particle size. These results were obtained from a calculation using the properties of TiO_2 with a filling fraction of 36 per cent. It shows that earlier measurements of anomalously low values of the diffusion coefficient in TiO_2 samples by Drake and Genack (1989) were most probably due to resonant scattering, reducing the transport speed and hence the diffusion coefficient, and not to the onset of Anderson localization. Subsequently, these calculations were improved by Busch and Soukoulis (1996) and Soukoulis and Datta (1994) to also be valid for higher filling fractions more appropriate to describe experiments. Using a combination of time-resolved transmission measurements (see below) and coherent backscattering measurements, Störzer, Aegerter and Maret (2006) measured the transport speed directly for a number of samples with different sizes. These measurements clearly show resonant reductions in the transport speed. The results are shown in Figure 27 and compared

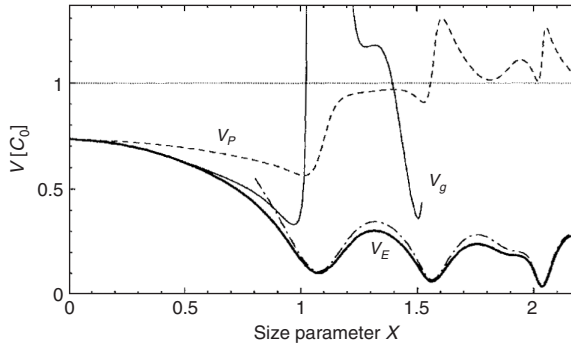

FIGURE 26 Calculation of the transport velocity as a function of the size parameter van Albada, van Tiggelen, Lagendijk and Tip (1991). The calculations were done for particles with a refractive index of 2.72, corresponding to that of TiO_2 in the rutile structure, and for a filling fraction of 3 per cent. Due to the fact that correlations between different scatterers are not taken into account in the calculation, the theory does not fully apply at high filling fractions. Reproduced with permission from van Albada, van Tiggelen, Lagendijk and Tip (1991) © 1991, American Physical Society

with the theoretical descriptions in the inset (upper line Soukoulis and Datta (1994), lower line van Albada, van Tiggelen, Lagendijk and Tip (1991)). There is reasonable agreement with the appropriate theory for higher filling fractions. In addition, these measurements show that the reduction in transport speed can be well separated from signatures of localization. Some of the samples studied here do show a non-exponential tail in the time-resolved transmission intensity as discussed below. However, these samples do not necessarily show a decrease in transport speed. This is because the Mie-resonances responsible for the increase in scattering cross-section (Mie, 1908) as well as resonant scattering are complemented by resonances in the structure factor, which influences only the scattering cross-section. Thus a suitable particle size and packing fraction can lead to a separation of the effects of localization and resonance scattering (Störzer, Aegerter and Maret, 2006).

In addition, resonant scattering was also observed in multiple scattering measurements on cold atoms (Labeyrie, Vaujour, Müller, Delande, Miniatura, Wilkowski and Kaiser, 2003), where a decrease in transport speed up to a factor of many orders of magnitude has been observed.

3.2.4 Statistical Features

As was discussed in the context of microwave experiments, the statistics of transmitted or reflected photons can also give valuable information about the samples and their possible localization properties. Due to its wave nature, multiply scattered light shows a characteristic interference

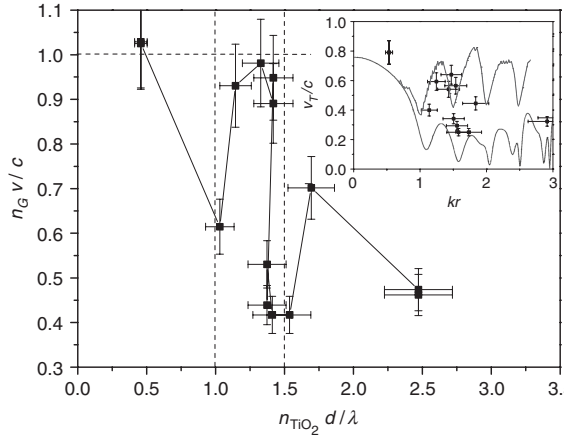

FIGURE 27 The transport velocity as measured from a combination of time-of-flight and backscattering measurements as obtained by Störzer, Aegerter and Maret (2006). The main figure shows the velocity relative to its expectation using the Garnett approach. This strongly overestimates the transport speed at particle sizes corresponding to integers of half the wavelength inside the scatterer. The inset shows the transport speed as a function of size parameter compared to theoretical expectations such as that shown in Figure 26 (lower line), and to calculations based on the model of Busch and Soukoulis (1996) that takes into account correlations between scatterers and thus should be applicable for high filling fractions (upper line). Reproduced with permission from Störzer, Aegerter and Maret (2006)

pattern known as speckle. The intensity of each speckle spot will be determined by the differing phase lags between photon paths. For a diffusive sample, the phase delay at differents point will be given by a Gaussian distribution, such that the corresponding intensity distribution is given by an exponential. This intensity distribution of the speckle pattern has been characterized by Wolf, Maret, Akkermans and Maynard (1988), where good agreement with the exponential decay of the probability has been found. Vellekoop, Lodahl and Lagendijk (2005) have measured the phase delay directly using interferometric methods (see Figure 28). This allows a study not only of the intensity distribution, but also of the phase distribution. From the width of this distribution, an independent measure of the diffusion coefficient can be found, which Vellekoop, Lodahl and Lagendijk (2005) find in good agreement with several other ways of determining D.

When photons are localized within a sample, the phase-delay distribution changes accordingly. Due to the presence of closed loops, there will be an increase in constructive interference of the different paths. In turn this leads to an intensity distribution with a non-exponential

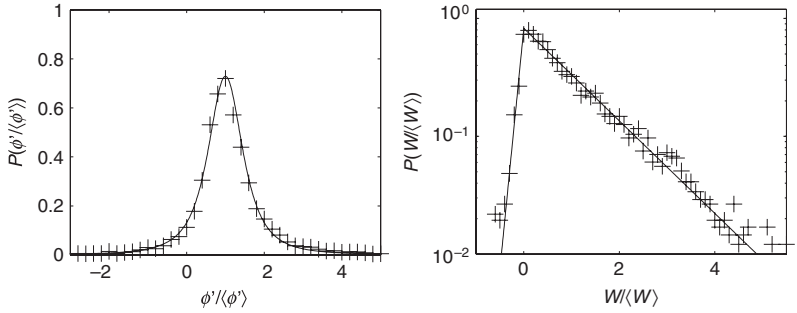

FIGURE 28 Distribution of the phase delay in a random sample. Left: delay time; right: delay time weighted by intensity. For classical samples, the width of these distributions yields a measure of the diffusion coefficient of light. In Vellekoop, Lodahl and Lagendijk (2005), this was done for TiO_2 particles of several sizes and a typical result is shown here. The determination of the diffusion coefficient in this way agrees very well with that from time-of-flight measurements. Reproduced with permission from Vellekoop, Lodahl and Lagendijk (2005) © 2005, American Physical Society

tail at high intensities (as well as a suppression at small intensities due to conservation of energy). This has been calculated in one-dimensional and quasi-one-dimensional systems (Nieuwenhuizen and van Rossum, 1995; Sebbah, Hu, Klosner and Genack, 2006). These calculations are in agreement with the results obtained from microwaves discussed above (Garcia and Genack, 1989), however, the situation in three-dimensional systems is less clear. There have, as yet, been no experimental findings of changed phase statistics close to Anderson localization. In addition, there are no explicit calculations for the phase distribution in a three-dimensional localizing sample.

3.3 Time-resolved Measurements

As we have seen above, static measurements of transmission or reflection are not readily suited for observing effects of strong localization. This is due to the fact that a simple loss of the number of photons in transmission in thick samples cannot distinguish localization from absorption. Therefore, one has to determine the phase of the photons as well. This can be done either via a quantification of the fluctuations, as discussed above, or via the time-resolved measurements we will discuss below. Since localization acts differently on photons that have spent different amounts of time inside the sample, localization and absorption can be separated in this case, as can be seen by the different functional dependencies implied by the effects. Absorption invariably leads to an exponential decrease also of the time-resolved intensity, while localization and its corresponding renormalization of the diffusion coefficient lead to a decay that is slower than exponential.

3.3.1 The Diffusion Coefficient

In a typical time-resolved measurement, the path-length distribution of photons inside a sample of finite thickness is obtained. This can be done either in transmission or in reflection. Due to the much faster time scale of the signal in reflection (most of the intensity is only delayed a time l^*/v), an experiment in transmission is much more feasible, although there have also been experiments in reflection (Johnson, Imhof, Bret, Rivas and Lagendijk, 2003). In the diffusion approximation, the path-length distributions can be calculated analytically (for a derivation see, for instance, Lenke and Maret (2000)). In transmission, one obtains:

$$T(t) \propto \sum_n (-1)^{n+1} \exp\left[-\left(\frac{n^2\pi^2 D}{L^2} + \frac{1}{\tau_{\text{abs}}}\right) t\right], \tag{10}$$

where τ_{abs} is the absorption length. Thus, for a sample of given length the time-resolved intensity is determined solely by D and τ_{abs}. These two parameters have very little covariance, as the time delay, until sizeable transmission through the sample is achieved, is solely determined by D, while the long-time behaviour is given by an exponential decay with a slope of $\pi^2 D/L^2 + 1/\tau_{\text{abs}}$.

In order to measure the time-resolved transmission, several types of setups have been used. Usually, a pulsed-laser system capable of producing picosecond pulses shines light on the sample. Behind the sample, a photodetector starts a clock that is subsequently stopped by a delayed reference pulse. For a more detailed description of such setups see, for instance, Watson, Fleury and McCall (1987) and Störzer, Gross, Aegerter and Maret (2006). For very thin samples, pulses on the scale of a few fs are needed, so that interferometric methods are needed for detection. This was done by Johnson, Imhof, Bret, Rivas and Lagendijk (2003) using samples of etched GaP (this will be discussed in more detail below in the context of time-resolved reflection measurements). Figure 29 shows the result of a measurement using a ps system (Störzer, Gross, Aegerter and Maret, 2006), in the case of a sample of TiO_2 particles of average diameter 540 nm at a wavelength of 590 nm. This sample has a value of $kl^* = 6.3(3)$ and thus shows purely diffusive behaviour as can be seen from the fit to Equation (10) shown as a thick solid line, which perfectly describes the data.

Due to the fact that time-resolved transmission thus allows a direct determination of the diffusion coefficient, many early experiments have looked for anomalously low values of D, or a thickness dependence of D (see e.g. Watson, Fleury and McCall (1987) and Drake and Genack (1989)). In these experiments, Drake and Genack (1989) found very low values of D and interpreted them as indications of the onset of localization

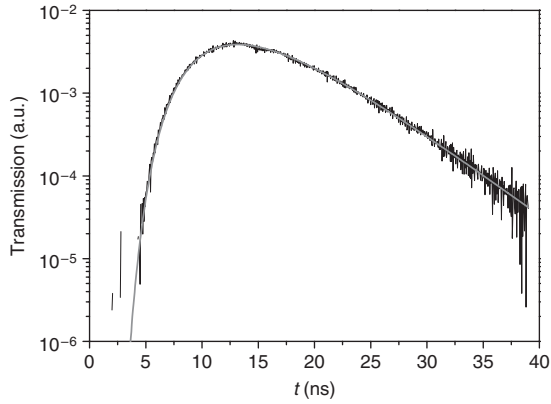

FIGURE 29 Time-resolved transmission for a classical sample with $kl^* = 6.3$ (data from Störzer, Gross, Aegerter and Maret (2006)). The thick solid line is a fit to classical diffusion theory through a slab of length L, which allows determination of the diffusion coefficient and the absorption length. There is little covariance between the two quantities as D determines the time lag before any photons are transmitted through the sample, while the absorption length only influences the slope of the exponential long-time tail.

(see Figure 30). However, due to resonance scattering, as discussed above and pointed out by van Albada, van Tiggelen, Lagendijk and Tip (1991), a low value of D does not necessarily imply a low value of l^* nor the onset of localization. This is because the reduction in transport velocity induced by the increased dwell time in resonance scattering will reduce the value of D obtained from time-of-flight measurements.

Similar information can also be gathered from a time-resolved measurement in reflection geometry. This setup presents additional experimental difficulties due to the much shorter time scales of the reflection signal. In reflection, most photons exit the sample after very few scattering events, therefore the peak in the time-resolved intensity is of the order of l/v, where l is the scattering mean free path. For samples close to the localization transition, i.e. with a mean free path comparable to the wavelength, this time is of the order of a few fs and thus very difficult to measure. After this peak, it can again be calculated in the diffusion approximation (see Johnson, Imhof, Bret, Rivas and Lagendijk (2003)) where the intensity decreases as

$$R(t) \propto \sum_n n^2 \exp\left[-\left(\frac{n^2\pi^2 D}{L^2} + \frac{1}{\tau_{\text{abs}}}\right)t\right]. \tag{11}$$

For short times this corresponds to a power-law decay with an exponent of 3/2, whereas at long times (the time scale of transmission)

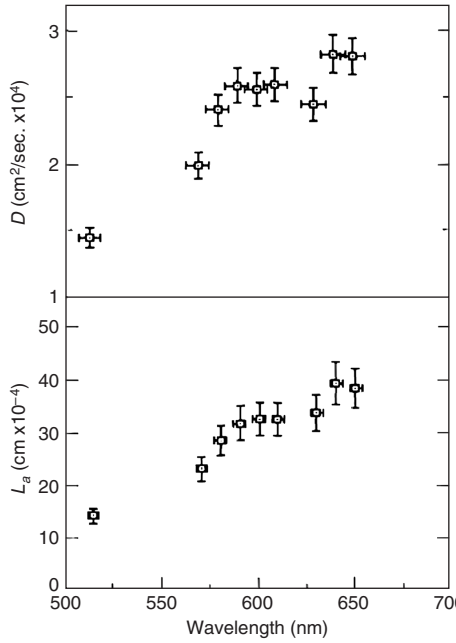

FIGURE 30 The diffusion coefficient and the absorption length of light through powders of TiO_2 as determined by time-of-flight measurements (Drake and Genack, 1989). The decrease of the diffusion coefficient with incident wavelength was interpreted as the onset of the localization transition, which predicts vanishing of the diffusion coefficient at a phase transition with kl^*, i.e. the wavelength. However, it has later been shown van Albada, van Tiggelen, Lagendijk and Tip (1991) that such a decrease is more likely to be due to an increased dwell time caused by resonant scattering of particles having roughly the same size as the wavelength of light. Reproduced with permission from Drake and Genack (1989) © 1989, American Physical Society

there is an exponential decay on the same time scale as in transmission measurements. Due to the time scale of the resulting intensity, measurements of time-resolved reflection need to be done with a fs-pulsed laser and the signal needs to be recorded interferometrically. In addition, the fact that most signals will be from photons which have only gone through a few scattering events, the signal-to-noise ratio will limit the time resolution to which reflection measurements can be performed. In spite of these differences, Johnson, Imhof, Bret, Rivas and Lagendijk (2003) have carried out measurements of time-resolved reflection on porous GaP samples with very small values of kl^*. Figure 31 clearly shows the initial power-law decay and the subsequent exponential decrease due to the finite sample and possible absorption.

Measurements of the diffusion coefficient from such time-resolved measurements, both in transmission and reflection, do show good

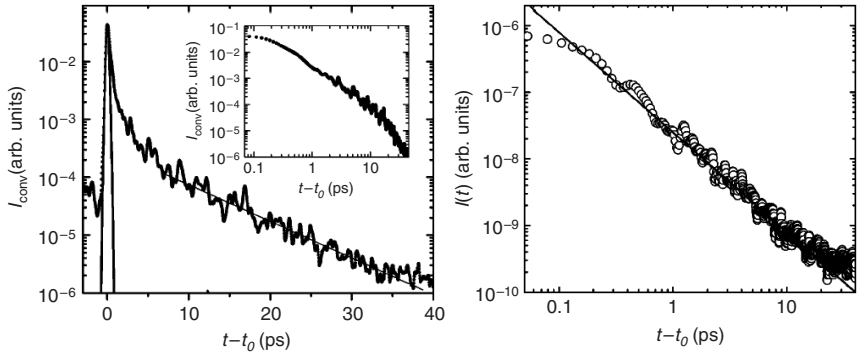

FIGURE 31 Time-resolved measurements of reflection (data from Johnson, Imhof, Bret, Rivas and Lagendijk (2003)). The left-hand panel presents the data on a logarithmic scale showing the exponential decrease at long times due to finite thickness and absorption. On the right the same data are shown on a double-logarithmic scale after deconvolution with the pulse shape. This demonstrates that at shorter times, the data can be described by a power-law decay with an exponent of 3/2 (straight line) in agreement with diffusion theory. Reproduced with permission from Johnson, Imhof, Bret, Rivas and Lagendijk (2003) © 2003, American Physical Society

agreement with determinations from the phase fluctuations as found by Vellekoop, Lodahl and Lagendijk (2005).

3.3.2 Spatially Dependent Diffusion Coefficient

Since time-resolved measurements of transmission or reflection are capable of determining the diffusion coefficient very accurately, it is also possible to employ such measurements in the search for a scale dependence of the diffusion coefficient. One of the hallmarks of localization, as discussed above, is that the diffusion coefficient becomes renormalized (Abrahams, Anderson, Licciardello and Ramakrishnan, 1979). This renormalization with the scale of the sample can be translated into a path-length dependence of the diffusion coefficient, as was first calculated by Berkovits and Kaveh (1987), at the critical point. Subsequently, they inserted this path-length dependence into the diffusion theory of time-resolved transmission (Berkovits and Kaveh, 1990). This changes the classical expectation (Equation (10)) to

$$T(t) \propto \sum_n (-1)^{n+1} \left(\frac{D(t)}{D_0}\right)^2 \exp\left[-\left(\frac{n^2\pi^2 D(t)}{L^2} + \frac{1}{\tau_{abs}}\right) t\right]. \qquad (12)$$

Similarly, a path-length dependence of the diffusion coefficient was used to calculate the influence of localization on the cone shape discussed

above (van Tiggelen, Lagendijk and Wiersma, 1995). Later investigations by some of these authors (Skipetrov and van Tiggelen, 2004, 2006) on self-consistent theory in open systems have explicitly calculated the effect of localization on time-resolved measurements. In reflection geometry, they find a change of the exponent of the power-law decay from 3/2 to 2 as the localization transition is crossed (Skipetrov and van Tiggelen, 2004). This will be extremely difficult to observe experimentally however. As discussed above, reflection measurements have to be done on short time scales and are limited by the signal-to-noise ratio due to high intensities at very short times. In addition, absorption and a finite sample will also lead to a decrease in intensity from the $t^{-3/2}$ power law, which will be exceedingly difficult to distinguish from the t^{-2} predicted by localization theory. In transmission, Skipetrov and van Tiggelen (2004) find a similar result as Berkovits and Kaveh (1990) in that the path-length dependence of the diffusion coefficient leads to a non-exponential tail in time-resolved transmission with a decreasing slope. In addition to Berkovits and Kaveh (1990) and Skipetrov and van Tiggelen (2004) also explicitly studied the effect of the dimensionality. Consistent with the scaling theory of Abrahams, Anderson, Licciardello and Ramakrishnan (1979), they find that in the quasi-one-dimensional case, effects of localization can already be observed above the transition (Skipetrov and van Tiggelen, 2004). With this it is possible, for instance, to describe the results on micro-wave transmission (Chabanov, Zhang and Genack, 2003) discussed above. In three-dimensional systems however, no signs of localization are observed above the transition at all (Skipetrov and van Tiggelen, 2006).

In Figure 32, we show time-resolved transmission measurements on a TiO_2 sample with a value of $kl^* \approx 2.5$(Störzer, Gross, Aegerter and Maret, 2006), the particles having a diameter of 250 nm. As can be seen, the transmission in this sample cannot be described by classical diffusion (Equation (10), shown by the dashed line) alone. There is a non-exponential decay with a decreasing slope as predicted by localization theory. This can be quantified in the same way as was done by Chabanov, Zhang and Genack (2003) as well as Skipetrov and van Tiggelen (2004), by taking the negative derivative of the log of the transmission data. This is shown in Figure 33 for several samples with varying values of kl^*. As can be seen, with decreasing kl^* there are increasing deviations from classical diffusion theory (solid line). This is, however, only a qualitative measure of possible signs of localization, and a more quantitative description is still needed. Unfortunately, the predictions of Skipetrov and van Tiggelen (2006) cannot be directly compared to the data, as the samples are much thicker than can be described theoretically. However, using the analytic description of Berkovits and Kaveh (1990) (Equation (12)), it is possible to obtain a path-length dependence of the diffusion coefficient from the

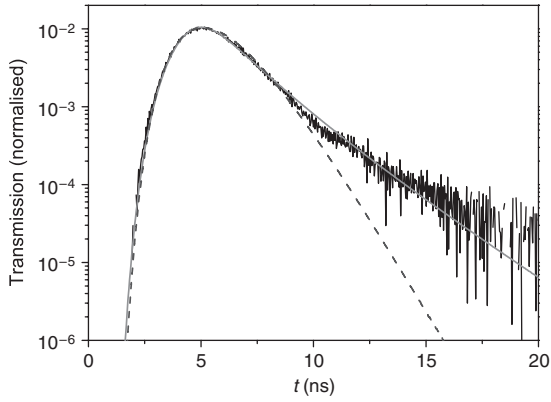

FIGURE 32 Time-resolved transmission of a localizing sample with $kl^* = 2.5$ (data from Störzer, Gross, Aegerter and Maret (2006)). As can be seen, the transmitted intensity at long times shows a non-exponential tail indicative of a renormalized diffusion coefficient (see Figure 33). In fact, the solid line is a fit to diffusion theory including a scale-dependent diffusion coefficient as done in Aegerter, Störzer and Maret (2006). For comparison, a fit to classical diffusion including absorption is shown by the dashed line

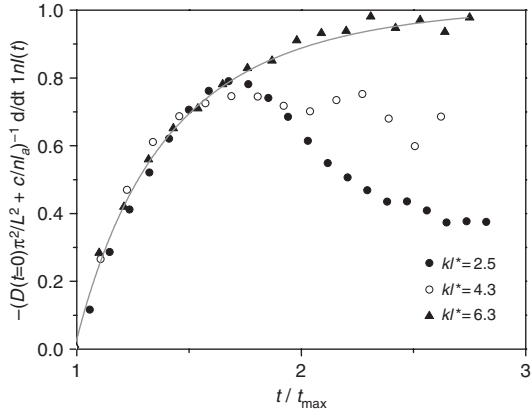

FIGURE 33 The long-time behaviour of time-of-flight measurements allows a direct determination of the spatial dependence of the diffusion coefficient. Taking the negative time-derivative of the logarithm of the transmitted intensity one obtains an effective diffusion coefficient, which should be constant at long times. This is shown here for three different samples, where the sample with $kl^* = 6.3$ agrees perfectly with diffusion theory and a constant diffusion coefficient. The sample with $kl^* = 2.5$ however shows a decrease of the diffusion coefficient at long times

data by way of a fit with $D(t)$. This is shown by the solid line in Figure 32, which describes the data reasonably well. The time dependence of $D(t)$

obtained from this fit is consistent with earlier simulation results by Lenke, Tweer and Maret (2002), where a self-attracting random walk was simulated and effective diffusion coefficients were determined. The result of these simulations in three dimensions shows that the diffusion coefficient is constant for some time, after which it decreases as $1/t$. This behaviour, the same as used to obtain the fit in Figure 32, can be physically explained from the fact that up to the localization length, roughly given by the size of the closed loops, the diffusion must be classical, as interference effects appear only after a closed loop has been traversed. At later times, the photons are localized to a specific region in space, such that $\langle r^2 \rangle$ tends towards a constant. Describing this behaviour with an effective $D(t)$ immediately leads to a dependence of $D(t) \propto 1/t$. This allows a quantitative discussion, not only of the time-resolved transmission experiments and the determination of the localization length discussed below, but also of the static transmission measurements discussed above.

The fact that Johnson, Imhof, Bret, Rivas and Lagendijk (2003) did not find a non-exponential decay in their time-resolved measurements while their samples had similar values of kl^* is probably due to the small thicknesses used in that study. As can be seen from Figure 32, in the TiO_2 samples the localization effects only start to appear after a few ns. This corresponds to roughly a million scattering events. Comparing this to the transmission data of Johnson, Imhof, Bret, Rivas and Lagendijk (2003), this is almost an order of magnitude bigger than their maximum time of flight (their maximum sample thickness is 20 μm). More quantitatively, this is connected to the size of the localization length discussed below.

3.3.3 The Localization Length

Given the phenomenological description of the diffusion coefficient based on the simulations of the self-attracting random walk discussed above (Lenke, Tweer and Maret, 2002), the deviations from the diffusion picture in time-resolved measurements can be quantified. In the localized state, the effective diffusion coefficient will decrease $\propto 1/t$, which corresponds to the limited extent of the photon cloud. On the other hand, above the transition the diffusion coefficient should be constant. This implies that a systematic study of the deviations from classical diffusion with decreasing kl^* should show a transition between these two asymptotic behaviours. In this case, the localization length would simply be given by $\sqrt{D_0 \tau_{\mathrm{loc}}}$, which however can only be determined as long as this length scale is smaller than the sample thickness.

Considering the predictions of one-parameter scaling theory however, the situation is somewhat more complicated. The fact that D is renormalized to be dependent on the sample thickness as $1/L$, has been translated to a path-length dependence by Berkovits and Kaveh (1990)

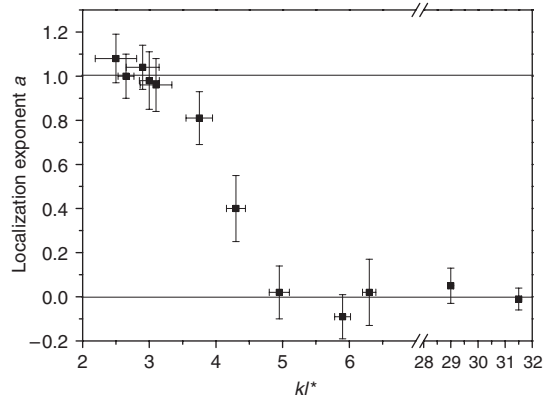

FIGURE 34 The scale dependence of the diffusion coefficient can be quantified by the exponent, a, with which D decreases as a function of time. Its value is plotted here as a function of kl^* (data from Aegerter, Störzer and Maret (2006)). As can be seen, above the transition to localization, the diffusion coefficient is constant as indicated by an exponent $a = 0$, whereas below $kl^* \approx 4$ it increases to $a = 1$, which corresponds to a localized state

to imply a path-length dependence as $D(t) \propto t^{-1/3}$. To take this into account, the time-of-flight measurements have been fitted with a power-law dependence of $D(t) \propto t^{-a}$ at long times (Aegerter, Störzer and Maret, 2006). In the approach to localization, this exponent increases from its classical value of zero to its localized value of unity. At the transition, even the exponent of $1/3$ can be observed, showing the critical point renormalization of the diffusion coefficient, see Figure 34. This plot also shows that the exponent is given by unity at low values of kl^*, corresponding to a localized state, while it is zero above the transition. This transition can be determined, from the dependence of the localization exponent in the figure, to be $kl_c^* \approx 4$.

The algebraic decay of the diffusion coefficient in the critical regime does somewhat complicate the determination of the localization length. Due to the fact that a classical behaviour can be obtained also from a change in the exponent, the localization length now has to be determined via $L^{1-a}\sqrt{D_0\tau_{\text{loc}}}^{a}$. In the limiting cases of $a = 1, a = 0$ this gives the same values as above, while giving an interpolation in the critical regime. The inverse of the localization length is the order parameter in the transition to localization. Therefore a systematic study of the localization length as a function of kl^* gives a description of the transition including the critical point and the critical exponent.

In Figure 35, this dependence is plotted with the localization length normalized to the sample thickness. For a finite sample, localization can only be observed if the localization length is smaller than the sample

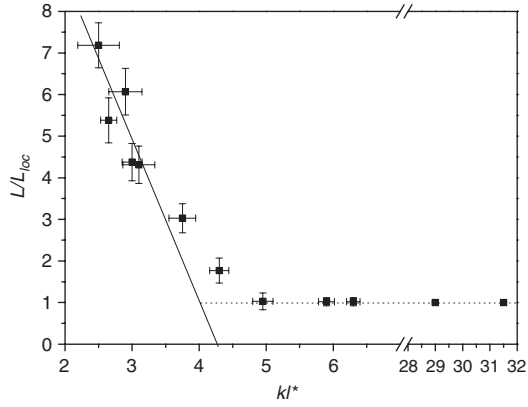

FIGURE 35 The dependence of the inverse localization length on the critical parameter kl^* (adapted from Aegerter, Störzer and Maret (2006)). Below a critical value of $kl_c^* \approx 4$, the localization length, as given by $\sqrt{D_0\tau_1}$, becomes smaller than the sample thickness, indicating the transition to a macroscopic population of localized states

thickness. Therefore, very thin samples having values of kl^* below the transition will not show effects of localization, and only very thick samples (with L far exceeding $100\,l^*$) can show the underlying transition. This is probably why the time-of-flight measurements of Johnson, Imhof, Bret, Rivas and Lagendijk (2003) are well described by classical diffusion in spite of the fact that their values of kl^* are close to or beyond the transition. Their samples, which consist of photoanodically etched GaP as already discussed above in the context of cone-tip measurements, are rather thin ($L \approx 40l^*$). This implies that the paths of the light traversed inside the sample are not sufficiently long to form enough closed loops and thus show localization.

3.3.4 Determination of the Critical Exponent

The systematic determination of the localization length for different samples around the localization transition also allows an experimental investigation of the critical exponent (Aegerter, Störzer and Maret, 2006). In this context, scaling theory (Abrahams, Anderson, Licciardello and Ramakrishnan, 1979) predicts a critical exponent $\nu < 1$, without specifying a precise value. As discussed above, an epsilon expansion in the dimension starting from the lower critical dimension ($d_l = 2$) yields a value of $1/2$ for the critical exponent (John, 1984), however due to the fact that the system considered here is fully three-dimensional, such a comparison cannot be considered precise. On the other hand, the fact, that above the upper critical dimension ($d_u = 4$) the mean-field value $\nu = 1/2$ is always obtained for the exponent of the order parameter in a second-

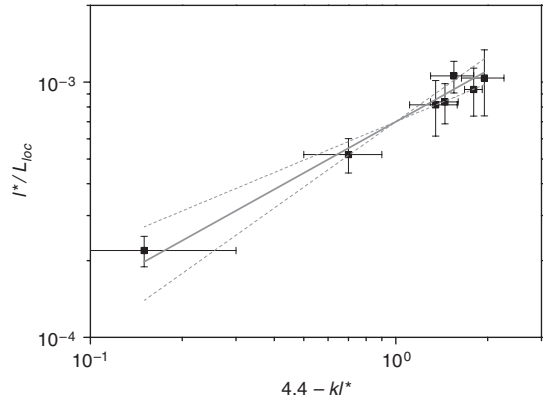

FIGURE 36 The inverse localization length as a function of the critical parameter $|kl^* - kl_c^*|$. As can be seen, the localization length diverges in the approach to a critical point at $kl_c^* = 4.4(2)$ with an exponent ν consistent with a value of 0.65(15) (solid line). This is in accordance with a mean-field argument for the value of the critical exponent but in contradiction to numerical simulations (MacKinnon and Kramer, 1981)

order phase transition (Schuster, 1978), would indicate that the value for a three-dimensional system should not be too far from these two limiting cases. In contrast, numerical evaluations of the Green–Kubo formalism consistently obtain a value of $\nu = 1.5$(MacKinnon and Kramer, 1981; Lambrianides and Shore, 1994; Rieth and Schreiber, 1997), which is not only inconsistent with the experimental data shown below, but also with one-parameter scaling theory (Abrahams, Anderson, Licciardello and Ramakrishnan, 1979). It should be noted however that these numerical investigations are carried out on quasi-periodic lattices. As such they thus do not necessarily conform to the nature of Anderson localization, which is fundamentally based on a completely disordered structure. This may explain the discrepancy with the analytic as well as the experimental results.

When plotting the inverse localization length against the critical parameter $|kl^* - kl_c^*|/kl^*$, Aegerter, Störzer and Maret (2006) obtained a divergence as shown in Figure 36, with a critical exponent of $\nu = 0.45(10)$. The above expression for the critical parameter was defined by Berkovits and Kaveh (1990), while John (1984) and others used the expression $|kl^* - kl_c^*|$. Using this latter critical parameter, the data yield a different exponent, namely $\nu = 0.65(15)$. The critical value of kl^* is not affected by the choice of critical parameter. Such an experimental determination can be used to test the different kinds of theoretical predictions discussed above. One notes that the result is consistent with the rather unspecific prediction of one-parameter scaling theory. Furthermore, it is in striking agreement with the result of the epsilon expansion, as well as the mean-

field prediction. This is somewhat surprising given that the experiments are carried out in a system of intermediate dimensionality, where both the epsilon expansion and the mean-field result should not explicitly hold. The numerical results finally are strongly inconsistent with the data, which might be due to the fact that the numerical results are obtained from quasi-periodic systems.

4. CONCLUSIONS AND OUTLOOK

Watching the light scattered back from an object can not only give a wealth of information on the scattering object, but also on some properties of light itself. As long as the scatterers are sufficiently random – and the samples thus opaque – the photonic analogue of the metal–insulator transition can be observed. Due to the fact that in this case there is no interaction between the diffusing particles (the photons, in contrast to the electrons in a metal), a theoretical treatment of photon localization is closer than that of electrons.

As we have seen however, great care has to be taken in the experimental investigation of photon localization. Absorption, resonant scattering or other external effects may well pose as localization in that they also produce an exponential decrease in transmission or a slowing down of transport, respectively. Therefore, investigations of localization have to concentrate on measures that are unaffected by absorption or transport speed, such as the speckle intensity distribution or time-resolved measurements. On the other hand, static measures are still useful, however one then needs an independent quantification of the absorption and the transport speed.

Using time-resolved measurements, Störzer, Gross, Aegerter and Maret (2006) have found clear indications of non-classical diffusion, which show all the hallmarks of localization and cannot be explained by the above artefacts. In fact, a quantitative description by Aegerter, Störzer and Maret (2006) of these data with qualitative localization theory not only finds localized states as given by a constant $\langle r^2 \rangle$, but can also describe the thickness dependence of the static transmission over twelve orders of magnitude without a single adjustable parameter. However, these measurements cannot provide evidence for the interference nature of the effect. For this purpose, measurements affecting the phase of the propagating photons would be necessary. In this context, it is useful to remember the work of Erbacher, Lenke and Maret (1993) and Golubentsev (1984), showing that weak localization can be destroyed by applying a strong magnetic field to a Faraday-active multiple-scattering medium. Using the same approach, it might be possible to add a Faraday-active material to a sample showing localization and apply a strong magnetic field. A destruction of the non-exponential tail in this case would clearly

show the interference nature of the effect and thus Anderson localization. Work to this effect is under way.

UNCITED REFERENCES

Fraden and Maret, 1990, Genack, 1987, Genack and Garcia, 1991, John, 1985, John, 1987, Rivas, Sprik, Lagendijk, Noordam and Rella, 2001, Schuurmans, Vanmaekelbergh, van de Lagemaat and Lagendijk, 1999, van Tiggelen, Lagendijk, Tip and Reiter, 1991, van Tiggelen, Wiersma and Lagendijk, 1995, Wiersma, 1995 and Wiersma, Gómez Rivas, Bartolini, Lagendijk and Righini, 1999.

ACKNOWLEDGEMENTS

We would like to thank all the current and previous members of the localization team in Konstanz/Strasbourg/Grenoble for their efforts over the years in studying multiple scattering. Without their work many results presented here would not have been possible. In particular, we thank M. Störzer, S. Fiebig, W. Bührer, P. Gross, R. Tweer, R. Lenke, R. Lehner, C. Eisenmann, D. Reinke, U. Mack, F. Scheffold, F. Erbacher, and P.E. Wolf.

In addition we would like to thank many colleagues for valuable discussions on pertinent questions as well as for making available some of their data to be presented here. These are E. Akkermans, N. Borisov, M. Fuchs, A.Z. Genack, M.D. Havey, R. Kaiser, A. Lagendijk, R. Maynard, G. Montambaux, M. Noginov, J. Pendry, P. Sebbah, P. Sheng, S.E. Skipetrov, H. Stark, B. van Tiggelen, and D.S. Wiersma.

Finally, this work is funded (2008) by the International Research Training Group "Soft Condensed Matter Physics of Model Systems" by the DFG and the Centre of Applied Photonics jointly financed by Ministry of Science, Research and Arts of Baden-Württemberg as well as the University of Konstanz. We are very grateful for their contributions.

REFERENCES

Abrahams, E., Anderson, P. W., Licciardello, D. and Ramakrishnan, T. V. (1979). Scaling theory of localization: Absence of quantum diffusion in two dimensions. *Phys. Rev. Lett.*, 42, 673–676.

Aegerter, C. M., Störzer, M. and Maret, G. (2006). Experimental determination of critical exponents in Anderson localization of light. *Europhys. Lett.*, 75, 562–568.

Aegerter, C. M., Störzer, M. and Maret, G. (2007). Observation of Anderson localization of light in bulk 3D systems, J. Opt. Soc. Am. (in press).

Akkermans, E., Wolf, P. E. and Maynard, R. (1986). Coherent backscattering of light by disordered media: Analysis of the peak line shape. *Phys. Rev. Lett.*, 56, 1471–1474.

Akkermans, E., Wolf, P. E., Maynard, R. and Maret, G. (1988). Theoretical study of the coherent backscattering of light by disordered media. *J. de Physique (France)*, 49, 77–98.

Akkermans, E. and Montambaux, G. (2006). *Mesoscopic Physics of Electrons and Photons*. Cambridge University Press.
Altshuler, B. L. and Lee, P. A. (1988). Disordered electronic systems. *Phys. Today*, (December), 36.
Anderson, P. W. (1958). Absence of diffusion in certain random lattices. *Phys. Rev.*, 109, 1492–1505.
Anderson, P. W. (1985). The question of classical localization: A theory of white paint? *Phil. Mag. B*, 52, 505–509.
Bayer, G. and Niederdränk, T. (1993). Weak localization of acoustic waves in strongly scattering media. *Phys. Rev. Lett.*, 70, 3884–3887.
Bergmann, G. (1984). Weak-localisation in thin films. *Phys. Rep.*, 107, 1–58.
Berkovits, R. and Kaveh, M. (1987). Backscattering of light near the optical Anderson transition. *Phys. Rev. B*, 36, 9322–9325.
Berkovits, R. and Kaveh, M. (1990). Propagation of waves through a slab near the Anderson transition: A local scaling approach. *J. Phys.: Condens. Mater.*, 2, 307–321.
Bidel, Y., Klappauf, B., Bernard, J. C., Delande, D., Labeyrie, G., Miniatura, C., Wilkowski, D. and Kaiser, R. (2002). Coherent light transport in a cold strontium cloud. *Phys. Rev. Lett.*, 88, 203902. 1–4.
Bryant, H. C. and Jarmie, N. (1974). The glory. *Sci. Am.*, 231 (1), 60–71.
Busch, K. and Soukoulis, C. M. (1996). Transport properties of random media: An energy-density CPA approach. *Phys. Rev. B*, 54, 893–899.
Campillo, M. and Paul, A. (2003). Long-range correlations in the diffuse seismic coda. *Science*, 299, 547–549.
Chabanov, A. A., Stoytchev, M. and Genack, A. Z. (2000). Statistical signatures of photon localization. *Nature (London)*, 404, 850–853.
Chabanov, A. A. and Genack, A. Z. (2001). Statistics of dynamics of localized waves. *Phys. Rev. Lett.*, 87, 153901. 1–4.
Chabanov, A. A., Zhang, Z. Q. and Genack, A. Z. (2003). Breakdown of diffusion in dynamics of extended waves in mesoscopic media. *Phys. Rev. Lett.*, 90, 203903. 1–4.
Cheung, S. K., Zhang, X., Zhang, Z. Q., Chabanov, A. A. and Genack, A. Z. (2004). Impact of weak localization in the time domain. *Phys. Rev. Lett.*, 92, 173902. 1–4.
Clément, D., Varón, A. F., Hugbart, M., Retter, J. A., Bouyer, P., Sanchez-Palencia, L., Gangardt, D. M., Shlyapnikov, G. V. and Aspect, A. (2005). *Phys. Rev. Lett.*, 95, 170409. 1–4.
Descartes, R. (1637), Discours de la Méthode Pour Bien Conduire Sa Raison et Chercher la Vérité dans les Sciences (second appendix) La Dioptrique.
Drake, J. M. and Genack, A. Z. (1989). Observation of nonclassical optical diffusion. *Phys. Rev. Lett.*, 63, 259–262.
Erbacher, F. A., Lenke, R. and Maret, G. (1993). Multiple light scattering in magneto-optically active media. *Europhys. Lett.*, 21, 551–557.
Faraday, M. (1846). On the magnetization of light and the illumination of magnetic lines of force. *Phil. Trans. Roy. Soc.*, 136, 1–20.
Fiebig, S., Aegerter, C. M., Bührer, W., Störzer, M., Montambaux, G., Akkermans, E. and Maret, G. (2007). Conservation of energy in coherent backscattering of light (to be published).
Fraden, S. and Maret, G. (1990). Multiple light scattering from concentrated, interacting suspensions. *Phys. Rev. Lett.*, 65, 512–515.
Fraser, A. B. (1994). The sylvanshine: retroreflection from dew-covered trees. *Appl. Opt.*, 33, 4539–4547.
Garcia, N. and Genack, A. Z. (1989). Crossover to strong intensity correlation for microwave radiation in random media. *Phys. Rev. Lett.*, 63, 1678–1981.
Garnett, J. C. M. (1904). Colours in metal glasses and in metallic films. *Phil. Trans. R. Soc. A*, 203, 385–420.
Gehrels, T. (1956). Photometric studies of asteroids; V. The lightcurve and phase function of 20 Massalia. *Astrophys. J.*, 123, 331–338.

Genack, A. Z. (1987). Optical transmission in disordered media. *Phys. Rev. Lett.*, 58, 2043–2046.
Genack, A. Z. and Garcia, N. (1991). Observation of photon localization in a three-dimensional disordered system. *Phys. Rev. Lett.*, 66, 2064–2067.
Golubentsev, A. A. (1984). Suppression of interference effects in multiple scattering of light. *Sov. Phys. JETP*, 59, 26–32.
Gross, P. (2005). Coherent backscattering close to the transition to strong localization of light, Diploma Thesis, Univ. of Konstanz.
Gross, P., Störzer, M., Fiebig, S., Clausen, M., Maret, G. and Aegerter, C. M. (2007). A precise method to determine the angular distribution of backscattered light to high angles. *Rev. Sci. Instr.*, 78, 033105.
Hapke, B. W., Nelson, R. M. and Smythe, W. D. (1993). The opposition effect of the moon: the contribution of coherent backscattering. *Science*, 260, 509–511.
Hikami, S. (1981). Anderson localization in a nonlinear-σ-model representation. *Phys. Rev. B*, 24, 2671–2679.
Igarashi, J.-I. (1987). Coherent backscattering of neutrons. *Phys. Rev. B*, 35, 8894–8897.
Ioffe, A. F. and Regel, A. R. (1960). Non-crystalline, amorphous and liquid electronic semiconductors. *Progr. Semicond.*, 4, 237–291.
Ishimaru, A. and Tsang, L. (1988). Backscattering enhancement of random discrete scatterers of moderate sizes. *J. Opt. Soc. Am. A*, 5 (2), 228–236.
John, S. (1984). Electromagnetic absorption in a disordered medium near a photon mobility edge. *Phys. Rev. Lett.*, 53, 2169–2172.
John, S. (1985). Localization and absorption of waves in a weakly dissipative disordered medium. *Phys. Rev. B*, 31, 304–309.
John, S. (1987). Strong localization of photons in certain disordered dielectric superlattices. *Phys. Rev. Lett.*, 58, 2486–2489.
Johnson, P. M., Imhof, A., Bret, B. P. J., Rivas, J. G. and Lagendijk, A. (2003). Time resolved pulse propagation in a strongly scattering material. *Phys. Rev. E*, 68, 016604. 1–9.
Jonckheere, T., Müller, C. A., Kaiser, R., Miniatura, C. and Delande, D. (2000). Multiple scattering of light by atoms in the weak localization regime. *Phys. Rev. Lett.*, 85, 4269–4272.
Kirkpatrick, T. R. (1985). Localization of acoustic waves. *Phys. Rev. B*, 31, 5746–5755.
Klitzing, K. v., Dorda, G. and Pepper, M. (1980). New method for high-accuracy determination of the fine-structure constant based on quantized Hall resistance. *Phys. Rev. Lett.*, 45, 494–497.
Kogan, E., Kaveh, M., Baumgartner, R. and Berkovits, R. (1993). Statistics of waves propagating in a random medium. *Phys. Rev. B*, 48, 9404–9407.
Kogan, E. and Kaveh, M. (1995). Random-matrix theory approach to the intensity distributions of waves propagating in a random medium. *Phys. Rev. B*, 52, R3813–R3815.
Kuga, Y. and Ishimaru, A. (1984). Retroreflectance from a dense distribution of spherical particles. *J. Opt. Soc. Am. A*, 1 (8), 831–835.
Kuhn, R. C., Miniatura, C., Delande, D., Sigwarth, O. and Müller, C. A. (2005). Localization of matter waves in two-dimensional disordered optical potentials. *Phys. Rev. Lett.*, 95, 250403. 1–4.
Kupriyanov, D. V., Sokolov, I. M., Kulatunga, P., Sukenik, C. I. and Havey, M. D. (2003). Coherent backscattering of light in atomic systems: application to weak localization in an ensemble of cold alkali-metal atoms. *Phys. Rev. A*, 67, 013804. 1–13.
Labeyrie, G., de Tomasi, F., Bernard, J.-C., Müller, C. A., Miniatura, Ch. and Kaiser, R. (1999). Coherent backscattering of light by cold atoms. *Phys. Rev. Lett.*, 83, 5266–5269.
Labeyrie, G., Delande, D., Müller, C. A., Miniatura, C. and Kaiser, R. (2003). Coherent backscattering of light by cold atoms: Theory meets experiment. *Europhys. Lett.*, 61, 327–333.
Labeyrie, G., Vaujour, E., Müller, C. A., Delande, D., Miniatura, C., Wilkowski, D. and Kaiser, R. (2003). Slow diffusion of light in a cold atomic cloud. *Phys. Rev. Lett.*, 91, 223904. 1–4.
Lagendijk, A., Vreeker, R. and de Vries, P. (1989). Influence of internal reflection on diffusive transport in strongly scattering media. *Phys. Lett. A*, 136, 81–88.

Lambrianides, P. and Shore, H. B. (1994). Numerical-scaling experiments in Anderson localization. *Phys. Rev. B*, 50, 7268–7271.
Larose, E., Margerin, L., van Tiggelen, B. A. and Campillo, M. (2004). Weak localization of seismic waves. *Phys. Rev. Lett.*, 93, 048501. 1–4.
Laughlin, R. B. (1983). Anomalous quantum Hall effect: an incompressible quantum fluid with fractionally charged excitations. *Phys. Rev. Lett.*, 50, 1395–1398.
Lee, P. A. and Ramakrishnan, T. V. (1985). Disordered electronic systems. *Rev. Mod. Phys.*, 57, 287–337.
Lenke, R. and Maret, G. (2000). Magnetic field effects on coherent backscattering of light. *Europ. Phys. J. B.*, 17, 171–185.
Lenke, R., Lehner, R. and Maret, G. (2000). Magnetic-field effects on coherent backscattering of light in case of Mie spheres. *Europhys. Lett.*, 52, 620–626.
Lenke, R. and Maret, G. (2000). Multiple scattering of light: coherent backscattering and transmission. In Brown, W. and Mortensen, K. (eds), *Scattering in polymeric and colloidal systems*. Gordon and Breach Scientific, New York, chap 1.
Lenke, R., Mack, U. and Maret, G. (2002). Comparison between "the Glory" and coherent backscattering of light in turbid media. *J. Opt. A: Pure Appl. Opt.*, 4, 309–314.
Lenke, R., Eisenmann, C., Reinke, D. and Maret, G. (2002). Measurement of the magneto-optical correlation length in turbid media. *Phys. Rev. E*, 66, 056610. 1–4.
Lenke, R., Tweer, R. and Maret, G. (2002). Coherent backscattering and localization in a self-attracting random walk model. *Eur. Phys. J. B*, 26, 235–240.
Lye, J. E., Fallani, L., Modugno, M., Wiersma, D. S., Fort, C. and Inguscio, M. (2005). Bose–Einstein condensate in a random potential. *Phys. Rev. Lett.*, 95, 070401. 1–4.
Maret, G. and Wolf, P. E. (1987). Multiple light scattering from disordered media. The effect of Brownian motion of scatterers. *Z. Phys.*, 65, 409–413.
MacKinnon, A. and Kramer, B. (1981). One-parameter scaling of localization length and conductance in disordered systems. *Phys. Rev. Lett.*, 47, 1546–1549.
MacKintosh, F. C. and John, S. (1988). Coherent backscattering of light in the presence of time-reversal-noninvariant and parity-nonconserving media. *Phys. Rev. B*, 37, 1884–1897.
Mie, G. (1908). Beiträge zur optik trüber medien, speziell kolloidaler metallösungen. *Ann. Phys.*, 25, 377–445.
Müller, C. A., Jonckheere, T., Miniatura, C. and Delande, D. (2001). Weak localization of light by cold atoms: the impact of quantum internal structure. *Phys. Rev. A*, 64, 053804.
Nieuwenhuizen, Th. M. and van Rossum, M. C. W. (1995). Intensity distributions of waves transmitted through a multiple scattering medium. *Phys. Rev. Lett.*, 74, 2674–2677.
Oetking, P. (1966). Photometric studies of diffusely reflecting surfaces with application to the brightness of the moon. *J. Geophys. Res.*, 71 (10), 2505–2513.
Pine, D. J., Weitz, D. A., Chaikin, P. M. and Herbolzheimer, E. (1998). Diffusing wave spectroscopy. *Phys. Rev. Lett.*, 60, 1134–1137.
Rieth, T. and Schreiber, M. (1997). The Anderson transition in three-dimensional quasiperiodic lattices: Finite-size scaling and critical exponent. *Z. Phys. B*, 104, 99–102.
Rikken, G. L. J. A. and van Tiggelen, B. A. (1996). Observation of magneto-transverse light diffusion. *Nature (London)*, 381, 54–56.
Rivas, J. G., Sprik, R., Lagendijk, A., Noordam, L. D. and Rella, C. W. (2000). Mid-infrared scattering and absorption in Ge powder close to the Anderson localization transition. *Phys. Rev. E*, 62, R4540–4543.
Rivas, J. G., Sprik, R., Lagendijk, A., Noordam, L. D. and Rella, C. W. (2001). Static and dynamic transport of light close to the Anderson localization transition. *Phys. Rev. E*, 63, 046613. 1–12.
Scheffold, F., Härtl, W., Maret, G. and Matijević, E. (1997). Observation of long-range correlations in temporal intensity fluctuations of light. *Phys. Rev. B*, 56, 10942–10952.
Scheffold, F. and Maret, G. (1998). Universal conductance fluctuations of light. *Phys. Rev. Lett.*, 81, 5800–5803.
Scheffold, F., Lenke, R., Tweer, R. and Maret, G. (1999). Localization or classical diffusion of light? *Nature (London)*, 398, 206–207.

Schuster, H. G. (1978). On a relation between the mobility edge problem schuster and an isotropic XY model. *Z. Phys.*, 31, 99–104.

Schuurmans, F. J. P., Megens, M., Vanmaekelbergh, D. and Lagendijk, A. (1999). Light scattering near the localization transition in macroporous GaP networks. *Phys. Rev. Lett.*, 83, 2183–2186.

Schuurmans, F. J. P., Vanmaekelbergh, D., van de Lagemaat, J. and Lagendijk, A. (1999). Strongly photonic macroporous gallium phosphide networks. *Science*, 284, 141–143.

Sebbah, P., Hu, B., Klosner, J. M. and Genack, A. Z. (2006). Extended quasimodes within nominally localized random waveguides. *Phys. Rev. Lett.*, 96, 183902. 1–4.

Shapiro, N. M., Campillo, M., Stehly, L. and Ritzwoller, M. H. (2005). High-resolution surface-wave tomography from ambient surface noise. *Science*, 307, 1615–1618.

Skipetrov, S. E. and van Tiggelen, B. A. (2004). Dynamics of weakly localized waves. *Phys. Rev. Lett.*, 92, 113901. 1–4.

Skipetrov, S. E. and van Tiggelen, B. A. (2006). Dynamics of Anderson localization in open 3D media. *Phys. Rev. Lett.*, 96, 043902. 1–4.

Snieder, R., Grêt, A., Douma, H. and Scales, J. (2002). Coda wave interferometry for estimating nonlinear behaviour in seismic velocity. *Science*, 295, 2253–2255.

Soukoulis, C. M. and Datta, S. (1994). Propagation of classical waves in random media. *Phys. Rev. B*, 49, 3800–3810.

Sparenberg, A., Rikken, G. L. J. A. and van Tiggelen, B. A. (1997). Observation of photonic magnetoresistance. *Phys. Rev. Lett.*, 79, 757–760.

Stellmach, Ch. (1998). Anderson-ocalization and High-frequency Induced Polarization of Ultracold Neutrons, PhD thesis, University of Heidelberg.

Stellmach, Ch., Abele, H., Boucher, A., Dubbers, D., Schmidt, U. and Geltenbort, P. (2000). On the Anderson-localization of ultra-cold neutrons. *Nucl. Instr. and Meth. A*, 440, 744–749.

Störzer, M., Gross, P., Aegerter, C. M. and Maret, G. (2006). Observation of the critical regime near Anderson localization of light. *Phys. Rev. Lett.*, 96, 063904. 1–4.

Störzer, M., Aegerter, C. M. and Maret, G. (2006). Reduced transport velocity of multiply scattered light due to resonant scattering. *Phys. Rev. E*, 73, 065602(R). 1–4.

Tsang, L. and Ishimaru, A. (1984). Backscatter enhancement of random discrete scatterers. *J. Opt. Soc. Am. A*, 1, 836–839.

van Albada, M. P. and Lagendijk, A. (1985). Observation of weak localization of light in a random medium. *Phys. Rev. Lett*, 55, 2692–2695.

van Albada, M. P., van Tiggelen, B. A., Lagendijk, A. and Tip, A. (1991). Speed of propagation of classical waves in strongly scattering media. *Phys. Rev. Lett.*, 66, 3132–3135.

van der Mark, M. B., van Albada, M. P. and Lagendijk, A. (1988). Light scattering in strongly scattering media: Multiple scattering and weak localization. *Phys. Rev. B*, 37, 3575–3592.

van Tiggelen, B. A., Lagendijk, A., Tip, A. and Reiter, G. F. (1991). Effect of resonant scattering on localization of waves. *Europhys. Lett.*, 15, 535–541.

van Tiggelen, B. A. (1995). Transverse diffusion of light in Faraday-active media. *Phys. Rev. Lett.*, 75, 422–424.

van Tiggelen, B. A., Wiersma, D. S. and Lagendijk, A. (1995). Self-consistent theory for the enhancement factor in coherent backscattering. *Europhys. Lett.*, 30, 1–7.

van Tiggelen, B. A., Lagendijk, A. and Wiersma, D. S. (2000). Reflection and transmission of waves near the localization threshold. *Phys. Rev. Lett.*, 84, 4333–4336.

Vellekoop, I. M., Lodahl, P. and Lagendijk, A. (2005). Determination of the diffusion constant using phase-sensitive measurements. *Phys. Rev. E*, 71, 056604. 1–11.

Vollhardt, D. and Wölfle, P. (1980). Diagrammatic, self-consistent treatment of the Anderson localization problem in $d \leq 2$ dimensions. *Phys. Rev. B*, 22, 4666–4679.

Watson, G. H., Fleury, P. A. and McCall, S. L. (1987). Searching for photon localization in the time domain. *Phys. Rev. Lett.*, 58, 945–948.

Wiersma, D. S. (1995). Light in Strongly Scattering and Amplifying Random Media, PhD thesis, Univ. of Amsterdam.

Wiersma, D. S., van Albada, M. P., van Tiggelen, B. A. and Lagendijk, A. (1995). Experimental evidence for recurrent multiple scattering events of light in disordered media. *Phys. Rev. Lett.*, 74, 4193–4196.

Wiersma, D. S., van Albada, M. P. and Lagendijk, A. (1995). An accurate technique to record the angular distribution of backscattered light. *Rev. Sci. Instr.*, 66, 5473–5476.

Wiersma, D. S., Bartolini, P., Lagendijk, A. and Righini, R. (1997). Localization of light in a disordered medium. *Nature (London)*, 390, 671–673.

Wiersma, D. S., Gómez Rivas, J., Bartolini, P., Lagendijk, A. and Righini, R. (1999). Reply to comment "Localization or classical diffusion of light?". *Nature (London)*, 398, 207.

Wigner, E. P. (1955). Lower limit for the energy derivative of the scattering phase shift. *Phys. Rev.*, 98, 145–147.

Wolf, P. E and Maret, G. (1985). Weak localization and coherent backscattering of photons in disordered media. *Phys. Rev. Lett.*, 55, 2696–2699.

Wolf, P. E., Maret, G., Akkermans, E. and Maynard, R. (1988). Optical coherent backscattering by random media: An experimental study. *J. Phys. (Paris)*, 49, 63–75.

Zhu, J. X., Pine, D. J. and Weitz, D. A. (1991). Internal reflection of diffusive light in random media. *Phys. Rev. A*, 44, 3948–3959.

Author Queries

Q1 (Page 1)

Please provide abstract and keywords.

Q2 (Page 56)

References Fraden and Maret (1990), Genack (1987), Genack and Garcia (1991), John (1985), John (1987), Rivas, Sprik, Lagendijk, Noordam and Rella (2001), Schuurmans, Vanmaekelbergh, van de Lagemaat and Lagendijk (1999), van Tiggelen, Lagendijk, Tip and Reiter (1991), van Tiggelen, Wiersma and Lagendijk (1995), Wiersma (1995) and Wiersma, Gomez Rivas, Bartolini, Lagendijk and Righini (1999) are provided but not cited in the text. Please cite these in text.